At the time of issue this report has not been published. Any author desiring to quote this paper should refer to it as "A paper of the Meteorological Research Committee (London), M.R.P. No. 841 by Mr. F.H. Bushby and Miss M.K. Hinds. A copy is available in the Library of the Meteorological Office".

M.R.P. 841

S.C.II/162

31st December, 1953.

AIR MINISTRY

METEOROLOGICAL RESEARCH COMMITTEE

The electronic computation of two series of 500 mb., 1000 mb., and 500-1000 mb. thickness forecast charts by application of the Sawyer-Bushby 2 parameter baroclinic model

by

F.H. Bushby and Mavis K. Hinds (Meteorological Office)

1. Introduction.

Several authors have recently suggested that the large-scale atmospheric motions could be predicted by the application of numerical methods of mathematical analysis to equations which represent the motion in various simplified models of the atmosphere. Charney and his colleagues at Princeton University have investigated the barotropic model atmosphere and Charney, Fjörtoft and von Neumann (1950) give the results of some 12 and 24 hour forecasts of the 500 mb. contour surface based on this model. More recently Charney and Phillips (1953) have given the results of some 12 and 24 hour forecasts based on the two-layer barotropic model. Alternatively, some of the baroclinic features of the atmosphere can be incorporated in a 2 parameter baroclinic model by assuming that the variation of the horizontal and vertical components of velocity with height is the same along all verticals. Eady (1952), Eliassen (1952), Sawyer and Bushby (1953) and Thompson (1953) have derived sets of equations which describe the motions in particular versions of this model.

The model of the atmosphere adopted by Sawyer and Bushby consists of a baroclinic fluid in which the thermal wind is constant in direction in any vertical column but not necessarily parallel to the wind direction at any level, and the thermal wind speed is assumed proportional to the pressure difference through the layer concerned. The atmosphere is considered bounded by two pressure surfaces across which the movement of the air is assumed to be negligible; one pressure surface $p = p_1$, corresponding to a level near the tropopause and one, $p = p_0$, corresponding to a level near the ground. The variation of the vertical motion with respect to pressure is assumed to be parabolic, and the geostrophic approximation is made after the horizontal divergence has been eliminated from the equations.

The present paper gives the result of 6, 12, 18 and 24 hour forecasts based on the Sawyer-Bushby model for two synoptic situations. The forecast charts are compared with the actual charts and an attempt is made to estimate the effect of computational instability and arbitrarily chosen boundary conditions on the answers.

/2.

2. The equations.

The state of motion in the Sawyer-Bushby model atmosphere is specified by the two parameters h_m, the height of the central pressure level of the layer (at $p = p_m$) and h', the thickness of the layer from p_0 to p_m. The method is one in which the instantaneous rates of change of h_m and h' are computed for time t and from these the values of h_m and h' for time $t + \delta t$. The process is then repeated n times and forecast charts are produced for time $t + n\delta t$.

Eliminating Π_m ($\Pi = dp/dt$, a measure of vertical motion) from the equations derived by Sawyer and Bushby, and neglecting the term representing the vertical advection of vorticity, the following equations can be derived for $\partial h_m/\partial t$ and $\partial h'/\partial t$:-

$$\nabla^2 \partial h_m/\partial t + J(h_m, \beta^2 g \ell^{-1} \nabla^2 h_m + \ell) + \tfrac{1}{3} J(h', \beta^2 g \ell^{-1} \nabla^2 h') = 0 \quad \ldots (1)$$

$$\nabla^2 \partial h'/\partial t + \frac{4g(\nabla^2 h_m + \ell^2/\beta^2 g)\{\beta^2 g \ell^{-1} J(h_m, h') + \partial h'/\partial t\}}{R A \Gamma (p_0 - p_1)}$$

$$+ J(h_m, \beta^2 g \ell^{-1} \nabla^2 h') + J(h', \beta^2 g \ell^{-1} \nabla^2 h_m + \ell) = 0 \quad \ldots (2)$$

where $A \equiv \frac{1}{2} \frac{p_0 + 3p_1}{p_0 - p_1} - \frac{4 p_0 p_1}{(p_0 - p_1)^2} \log_e \frac{2p_0}{p_0 + p_1}$,

∇^2 and J are the two dimensional Laplacian and Jacobian operators referred to rectangular Cartesian co-ordinates in the stereographic projection of the northern hemisphere on to a plane perpendicular to the earth's axis passing through the north pole; β is the magnification factor $\sec^2(\pi/4 - \theta/2)$, θ being the geographical latitude; g is the acceleration due to gravity; ℓ is the Coriolis parameter; R is the universal gas constant and Γ_p a measure of the departure of the lapse rate from the adiabatic given by $\Gamma_p = \frac{\partial T}{\partial p} - \gamma/g\ell$, γ being the appropriate wet or dry adiabatic lapse rate, ℓ the density and T the absolute temperature. Neglect of the terms involving the vertical advection of vorticity is justified by the small values of this term obtained in M.R.P. 790.

The following system of equations was used for the time integration process:-

$$H_{n+1} = h_{n-1} + 2(\partial H/\partial t)_n \, \delta t \quad \ldots\ldots\ldots\ldots (3)$$

$$h_{n+1} = h_n + \tfrac{1}{2}\left[(\partial H/\partial t)_n + (\partial H/\partial t)_{n+1}\right] \delta t \quad \ldots\ldots\ldots (4)$$

/where

where H_n represents the first approximation and h_n the second approximation to either h_m or h' at time $t + n\delta t$. Initially, as only values of h_m and h' are known at one instant of time, it was necessary to replace the centred difference of Equation (3) by the forward difference formula

$$H_1 = h_0 + \left(\partial h/\partial t\right)_0 \delta t \qquad \ldots\ldots\ldots\ldots (5)$$

It was decided to use Equations (3) and (4) instead of Equation (3) alone for the time integration procedure in an attempt to reduce the effect of computational instability.

The computations were carried out on LEO, an electronic computing machine owned by Messrs. J. Lyons and Co. The finite difference approximations to Equations (1) and (2) were solved for $\partial h_m/\partial t$ and $\partial h'/\partial t$ using the technique described by Bushby and Hinds (1953a and b). A grid of 18 x 14 points was used, but as two rings of points are lost in computing the finite difference approximations to the vorticity advection terms, Equations (1) and (2) are solved for a grid of 16 x 12 points including boundary points.

Due to limitations of storage space in LEO, it was impossible to keep the complete programme in the machine, and this slowed down the computation. The new values of h_m and h' were printed after each time step. The time spent in completing one cycle of the computations was 20 minutes: of this 5 minutes were spent in input, 5 minutes in output and 10 minutes in actual computation. To produce a forecast at time $t + n\delta t$ from initial data at time t would thus take $n/3$ hours if the intermediate results were printed, and $(n/4 + 1/12)$ hours if only the final results were printed.

In the present work the values of p_0 and p_1 were taken to be 1000 mb. and 200 mb. respectively. This would give p_m = 600 mb., a level for which charts are not normally available. h_m was therefore identified with the height of the 500 mb. surface and h' with the thickness of the 1000-500 mb. layer.

After consideration of previous computational results a constant value, 38°F. per 500 mb., was taken for Γ_p.

3. The space and time increments.

In order that the solution of the finite difference approximations to Equations (1) and (2) should closely approximate to the continuous solution, it is necessary that the space and time increments δs and δt must be small in comparison with the space and time scales of the large scale atmospheric systems. However, the smaller δs, the more grid points are necessary to cover a given area, and the computation time is increased. After some experimenting it was decided to use a value of δs which approximates to 162 statute miles in middle latitudes.

Apart from the aforementioned considerations it is also necessary to ensure that the small-scale irregularities in the field of h_m and h', of which there is inevitably a large distortion, do not amplify during the integration process. The computation is said to be unstable when such amplification takes place. Due to the complex nature of the equations involved it is extremely difficult to derive rigorously the conditions necessary for stability, but it is apparent that the ratio $\delta s/\delta t$ has to lie within certain limits.

/From

From general considerations, it was decided to commence the computations with δt equal to 2 hours. It can be seen from inspections of the results (Figs. 1-5) that the integration based on the initial data of 1500 G.M.T. 27.1.1952 was unstable after 18 hours. The distortions increased in amplitude by 24 hours but did not affect the region of the British Isles, for which a reasonable 24 hour forecast was computed.

During the integration based on the initial data of 1500 G.M.T. 14.3.1949 instability became apparent after 10 hours and considerable amplification and distortion over most of the chart had taken place by 12 hours. The computation was stopped and re-started from the 8 hour stage, using δt equal to 1 hour. The calculations then remained stable over the whole of the chart for the 24 hours (Figs. 6-10).

Charney et al (1950), when solving the barotropic equation using a centred difference formula for the time integration, derived the following approximate relationship

$$\frac{\delta s}{\delta t} \geqslant \sqrt{2}/\beta - v \quad \text{- - - - - - - - - - - (6),}$$

where v is the maximum particle speed in the forecast region, as giving a lower bound to the stability criterion. If the same relationship applied to the present set of equations, then with δt = 2 hours, the computations would become unstable if v were greater than 60 knots in middle latitudes. It is thought that the present method of time integration is more stable than the simple centred difference formula used by Charney et al (1950), but the problem of computational instability is at present being further investigated in the Forecast Research Division at Dunstable.

4. The boundary conditions.

A sufficient boundary condition for the solution of Equations (1) - (5) in a given region is that h_m, h', $\nabla^2 h_m$ and $\nabla^2 h'$ should be given along the boundary of that region. Thus when the finite difference approximations to Equations (1) - (5) are being solved, it is necessary to specify the values of h_m, h', $\nabla^2 h_m$ and $\nabla^2 h'$ at all grid points on the boundary (except corner points) or alternatively to specify the values of h_m and h' at all grid points on the boundary and at all grid points immediately exterior to the boundary. The second of these two alternatives was used in the present computations.

It was considered that the arbitrary boundary values would not affect the centre of the forecast region by the end of the forecast period. The actual boundary values assigned to h_m and h' have to be chosen quite arbitrarily, because unless one considers the whole of the northern hemisphere in order to make use of the observed fact that h_m and h' show little variation near the equator, there are no conclusive reasons for pre-determining the values of h_m and h' along the boundary. The following boundary values were chosen as they are quite simple and tend to smooth the field of h_m and h' in a direction normal to the boundary in the vicinity of the boundary.

The initial data used in the computations were the values of h_m and h' at the points of an 18 x 14 grid. This enabled the Poisson and Helmholtz Equations (1) and (2) to be solved for $\partial h_m/\partial t$ and $\partial h'/\partial t$ at 16 x 12 points including the boundary points at which values of $\partial h_m/\partial t$ and $\partial h'/\partial t$ were assumed zero. However in using Equations (3), (4) and (5)

/for

for the time integration, $\partial h_m/\partial t$ and $\partial h'/\partial t$ were taken as zero at the boundary points of the 18 x 14 grid but at the boundary points of the inner 16 x 12 grid $\partial h_m/\partial t$ and $\partial h'/\partial t$ were now taken equal to half the value at the immediate interior point except at the four corner points where a value of one quarter of the nearest interior point was used. The area covered by this 16 x 12 grid of points is that inside the curved boundary shown in Fig. 2b.

5. The results.

(a) Time-integration based on initial data for 1500 G.M.T. 27th January, 1952.

The initial charts on which this computation is based are shown in Figs. 1a and 1b. The situation was one in which there was a broad westerly flow across the North Atlantic at 500 mb., with large-amplitude troughs over eastern Canada and western Europe and an intermediate shallower trough south-east of Greenland. Surface and thickness patterns were also largely westerly over the Atlantic, but over western Europe the surface pressure gradient was flat and mainly cyclonic, there being a tongue of deep cold air down the North Sea into northern France.

During the ensuing twenty-four hours the cold trough over the North Sea moved slowly eastwards to Scandinavia and eastern Germany, the associated surface trough also moving away eastwards. The movements of this feature were well forecast, the axis of the 500 mb. trough being in almost the correct position on each of the forecast charts. The surface low pressure area was not, however, forecast to move far enough eastwards. Behind the base of the cold trough the ridge originally over the Bay of Biscay was forecast to intensify considerably and move eastwards to reach a position over northern Italy after twenty-four hours. The ridge moved as forecast for the first twelve hours but thereafter, possibly owing to the close proximity of the Alps, moved more north-eastwards than forecast. This is a particularly marked example of a circumstance in which an experienced forecaster would almost certainly use his knowledge of the topography to modify a forecast produced by numerical methods. The elongated frontal trough to the west of Ireland intensified and moved eastward over the British Isles slightly faster than forecast, but the axis of the warm ridge was correctly forecast to be over Great Britain after twenty-four hours. The separate low pressure centre forecast to develop in the lower end of the trough did in fact form at the point of occlusion shortly after the end of the forecast period.

The part of the forecast charts to the west of the British Isles has been considerably affected by computational instability and arbitrary choice of boundary values, the difficulties discussed in sections 3 and 4. During the forecast period the deep cold trough over eastern Canada moved eastwards across the boundary of the area involved in the computations. Since, however, the values of h_m and h' along this boundary were assumed to remain constant, the cold trough was assumed to remain back over America and an intense warm ridge was forecast to be thrown up ahead of it. This gave rise to very tight gradients just south of Greenland on the forecast charts and small, intense irregularities appear downstream on the forecast charts due to computational instability.

(b) Time-integration based on initial data for 1500 G.M.T. 14th March, 1949.

Figs. 6a and 6b show the initial charts used in this forecast. A large stationary depression is situated over the Baltic in a very slack

/thermal

thermal gradient, whilst a vigorous depression is approaching the southern tip of Greenland from the south-west. Between the two a considerable ridge extends northwards from the Azores high pressure area. There is a small wave-depression over southern England and a shallow low pressure area with an almost concentric cold pool south-west of Spain.

In this situation the movements of various pressure systems were quite well forecast, but the predictions of their development and intensity were considerably in error. It is particularly noticeable how similar the forecast and actual patterns are at 500 mb., the main errors in the forecast being the intensification of the 500 mb. ridge north of the Azores and the small trough west of Iceland.

During the twenty-four hours for which the forecast was made the wave depression moved rapidly away into Russia and was followed by a mobile ridge which spread down into southern England and France and was absorbed into the considerably enlarged Azores High. On the forecast charts the oscillation in the thickness pattern was predicted to intensify too much giving a very strong westerly thermal gradient over Iceland and northerly thermal gradient over the British Isles. This oscillation gave a very marked anticyclonic development area over the British Isles and in consequence the mobile ridge was forecast to develop into an extremely intense high pressure area with the Azores High as a ridge extension.

The depression approaching the tip of Greenland at the beginning of the period was forecast to split into two parts, a shallow low pressure area in the Davis Strait and a more intense depression moving north-eastward to Iceland. This movement actually occurred but the depression over Iceland was less deep than it was forecast to be.

Reducing the time-step to one hour appears to have removed most of the effects of computational instability and the western halves of the twenty-four hour forecast charts in this case are very much more in agreement with actuality than in the other case where two-hour time-steps were used throughout. It is possible that if one-hour time-steps had been used throughout all the effects of computational instability would have been removed.

(c) Correlation and regression coefficients.

Correlation coefficients have been calculated comparing computed changes with actual changes over 6, 12, 18 and 24 hour periods starting from the initial data. Regression coefficients were calculated for the best fitting straight lines giving the actual change (Y tens of feet) in terms of the computed change (X tens of feet) in the form

$$Y = bX + c \qquad \text{.....(7)}$$

In order to gain an indication of the adverse effects of computational instability and wrong boundary conditions on the western part of the forecast charts, correlation and regression coefficients were calculated both for the 16 x 12 grid of points over which the contour heights and thickness were forecast to change and also over the same area without the six westernmost columns of points.

/Table I.

Table I.

Correlation and regression coefficients of actual and computed height and thickness changes for forecast period beginning 1500 G.M.T. 27.1.52.

Forecast period ending	grid size	500 mb.			1000 mb.			1000-500 mb.		
		r	b	c	r	b	c	r	b	c
2100 G.M.T. 27.1.52	16x12	0.53	0.64	0.2	0.68	0.68	0.9	0.68	0.64	-0.5
	10x12	0.71	0.94	1.1	0.80	0.80	3.4	0.71	0.80	-0.5
0300 G.M.T. 28.1.52	16x12	0.41	0.43	3.6	0.35	0.47	-0.3	0.55	0.46	2.4
	10x12	0.82	0.98	9.2	0.71	0.67	6.0	0.77	0.78	-0.4
0900 G.M.T. 28.1.52	16x12	0.29	0.24	-0.9	0.33	0.46	-1.4	0.55	0.34	-0.4
	10x12	0.78	0.76	7.6	0.81	0.78	9.0	0.77	0.59	-0.5
1500 G.M.T. 28.1.52	16x12	0.05	0.04	3.0	0.22	0.29	-1.5	0.45	0.22	2.9
	10x12	0.83	0.78	12.7	0.78	0.81	11.0	0.77	0.56	2.6

r = correlation coefficient.

Table II.

Correlation and regression coefficients of actual and computed height and thickness changes for forecast period beginning 1500 G.M.T. 14.3.49.

Forecast period ending	grid size	500 mb.			1000 mb.			1000-500 mb.		
		r	b	c	r	b	c	r	b	c
2100 G.M.T. 14.3.49	16x12	0.79	0.94	-3.1	0.79	0.56	0.6	0.53	0.57	-1.8
	10x12	0.85	0.89	5.0	0.77	0.56	0.5	0.73	0.66	0.4
0300 G.M.T. 15.3.49	16x12	0.66	0.58	-3.0	0.81	0.59	0.7	0.78	0.82	-5.1
	10x12	0.84	0.83	-4.7	0.90	0.70	-2.2	0.85	0.80	-0.8
0900 G.M.T. 15.3.49	16x12	0.74	0.66	-7.5	0.77	0.54	-1.4	0.72	0.69	-5.1
	10x12	0.86	0.79	-9.0	0.89	0.61	-3.5	0.88	0.75	1.4
1500 G.M.T. 15.3.49	16x12	0.69	0.59	-9.7	0.76	0.47	-3.3	0.81	0.64	-4.4
	10x12	0.76	0.71	-13.3	0.83	0.52	-6.8	0.94	0.68	-0.1

The figures given in Tables I and II confirm what has been said in sections 5a and 5b. The most striking feature of Table I is the very high correlations obtained if the six westernmost columns of the grid are ignored. In Table II the correlations are fairly high even when these columns are included, but it will be noticed that the values of b are almost invariably lower than the corresponding correlation coefficients owing to the fact that many features on the charts were forecast to intensify too much.

/6.

6. Conclusions.

Although one must not generalise from two examples, in the two situations so far considered the equations describing the motion in the Sawyer-Bushby 2 parameter baroclinic model atmosphere give a fair representation of the motion in the real atmosphere for a 24 hour period in the regions not affected by computational instability and the arbitrary choice of boundary conditions.

References:

Bushby, F.H. and Hinds, M.K.	1953	(a) Air Ministry, Met. Res. Ctee., M.R.P. 790.
		(b) Air Ministry, Met. Res. Ctee., M.R.P. 794.
Charney, J.G., Fjörtoft, R. and von Neumann, J.	1950	Tellus, 2, p.237.
Charney, J.G. and Phillips, N.A.	1953	J. Met., 10, p.71.
Eady, E.T.	1952	Tellus, 4, p.157.
Eliassen, A.	1952	Tellus, 4, p.145.
Sawyer, J.S. and Bushby, F.H.	1953	J. Met., 10, p.54.
Thompson, P.D.	1953	Quart. J. R. Met. Soc., 79, p.51.

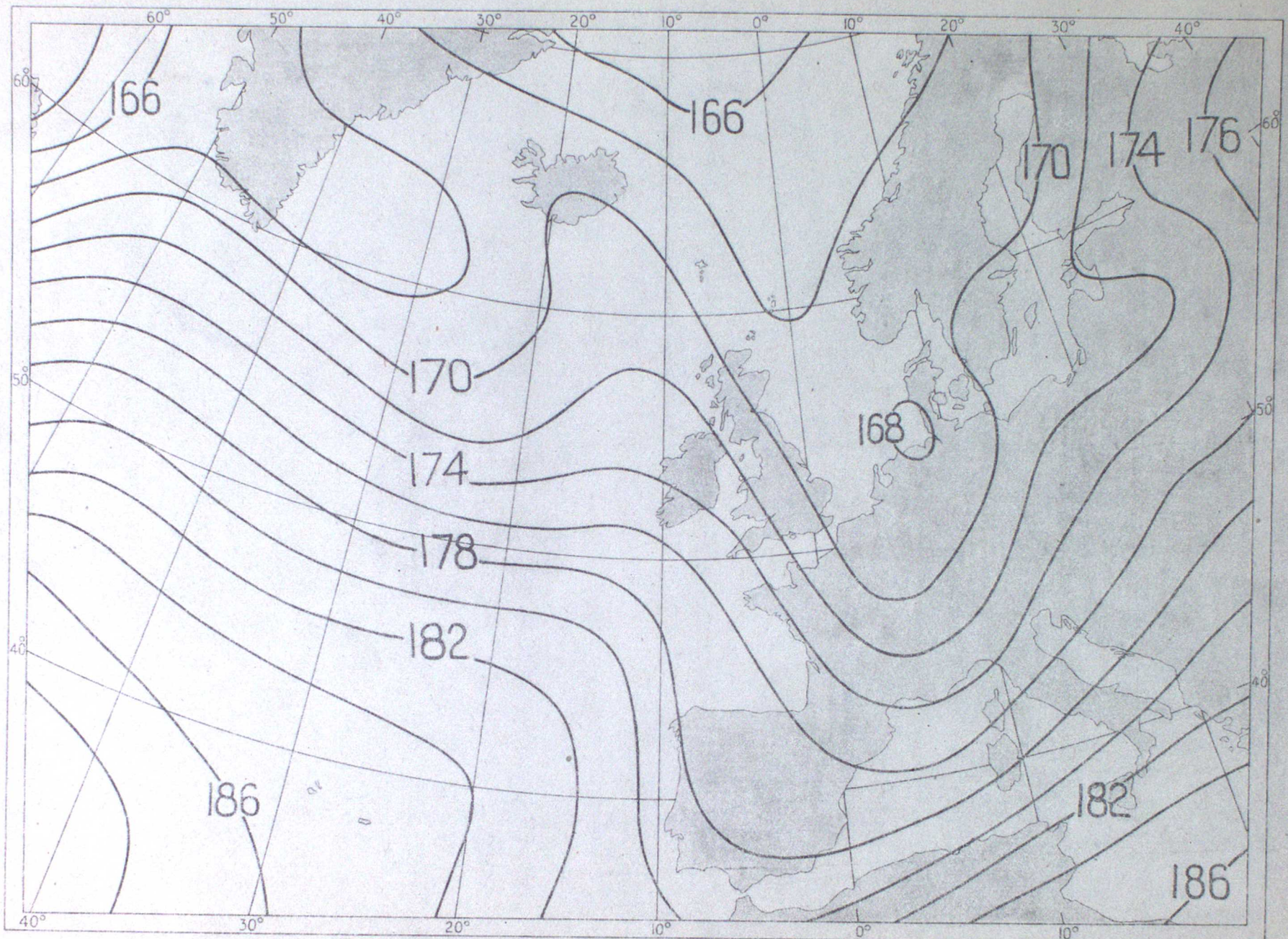

Fig. 1(a) Actual 500mb. contour chart for 1500 G.M.T. 27.1.52

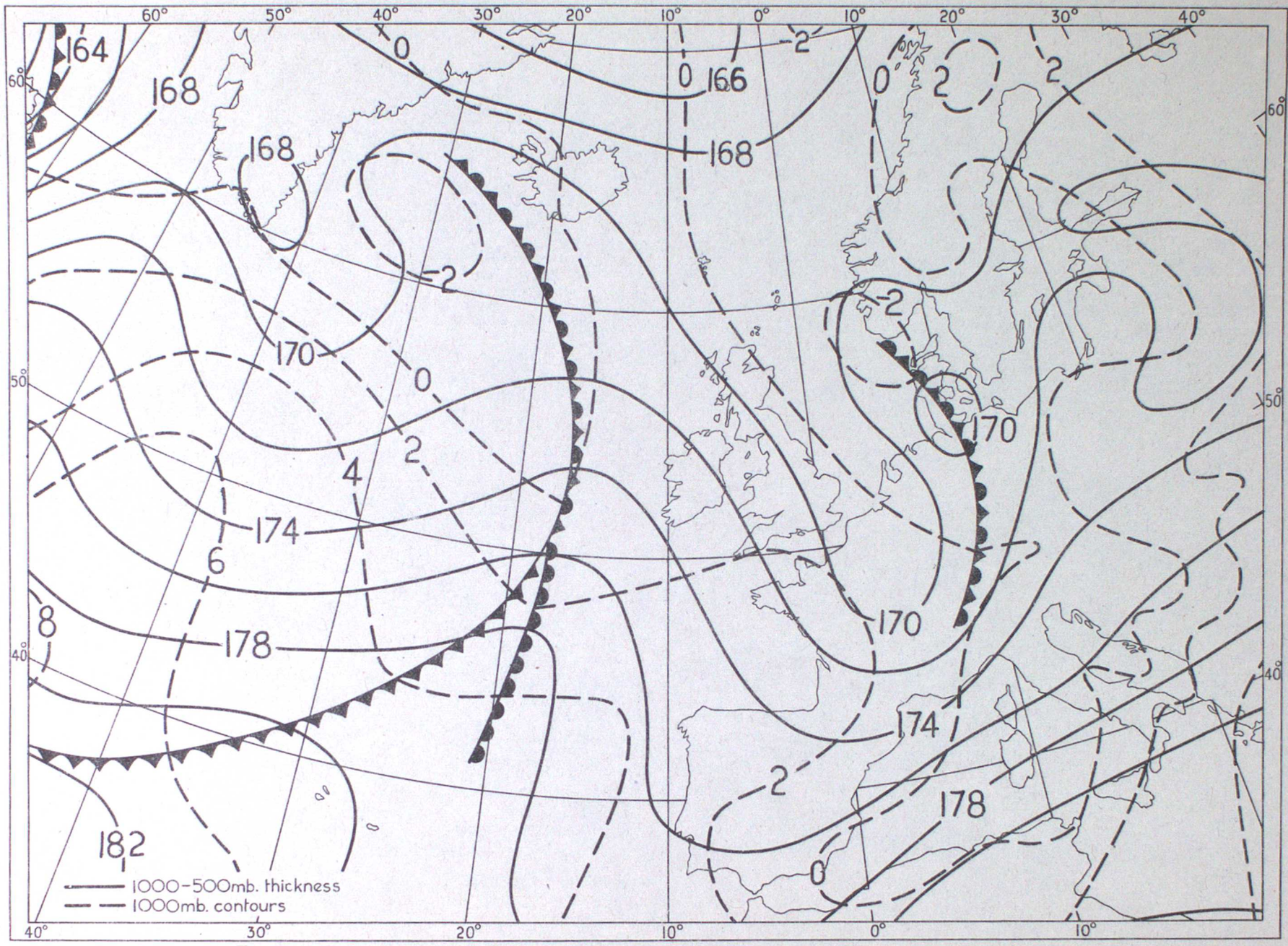

Fig. 1(b) Actual 1000–500mb. thickness and 1000mb. contours for 1500 G.M.T. 27.1.52

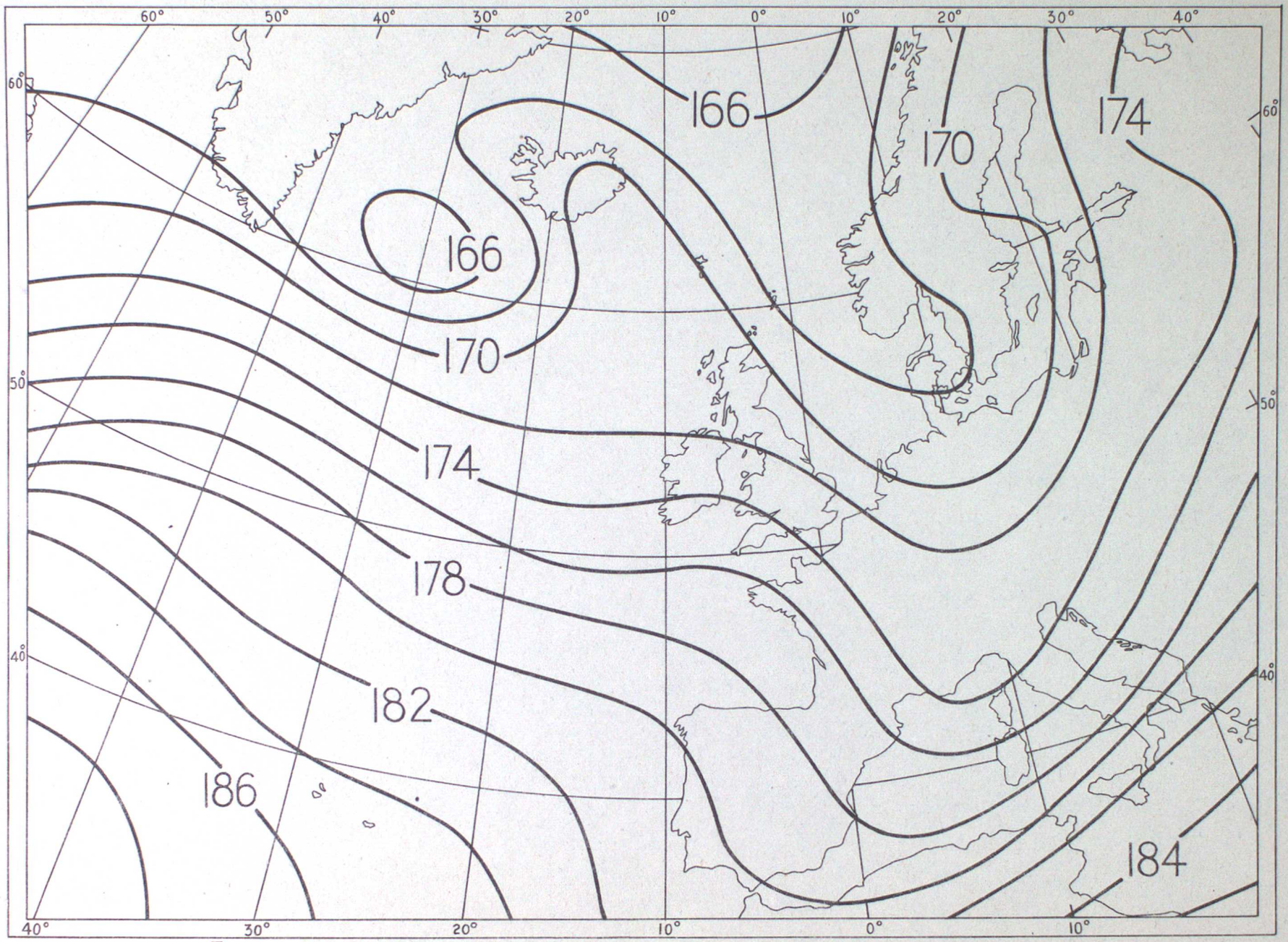

Fig. 2(a) Actual 500mb. contour chart for 2100 G.M.T. 27.1.52

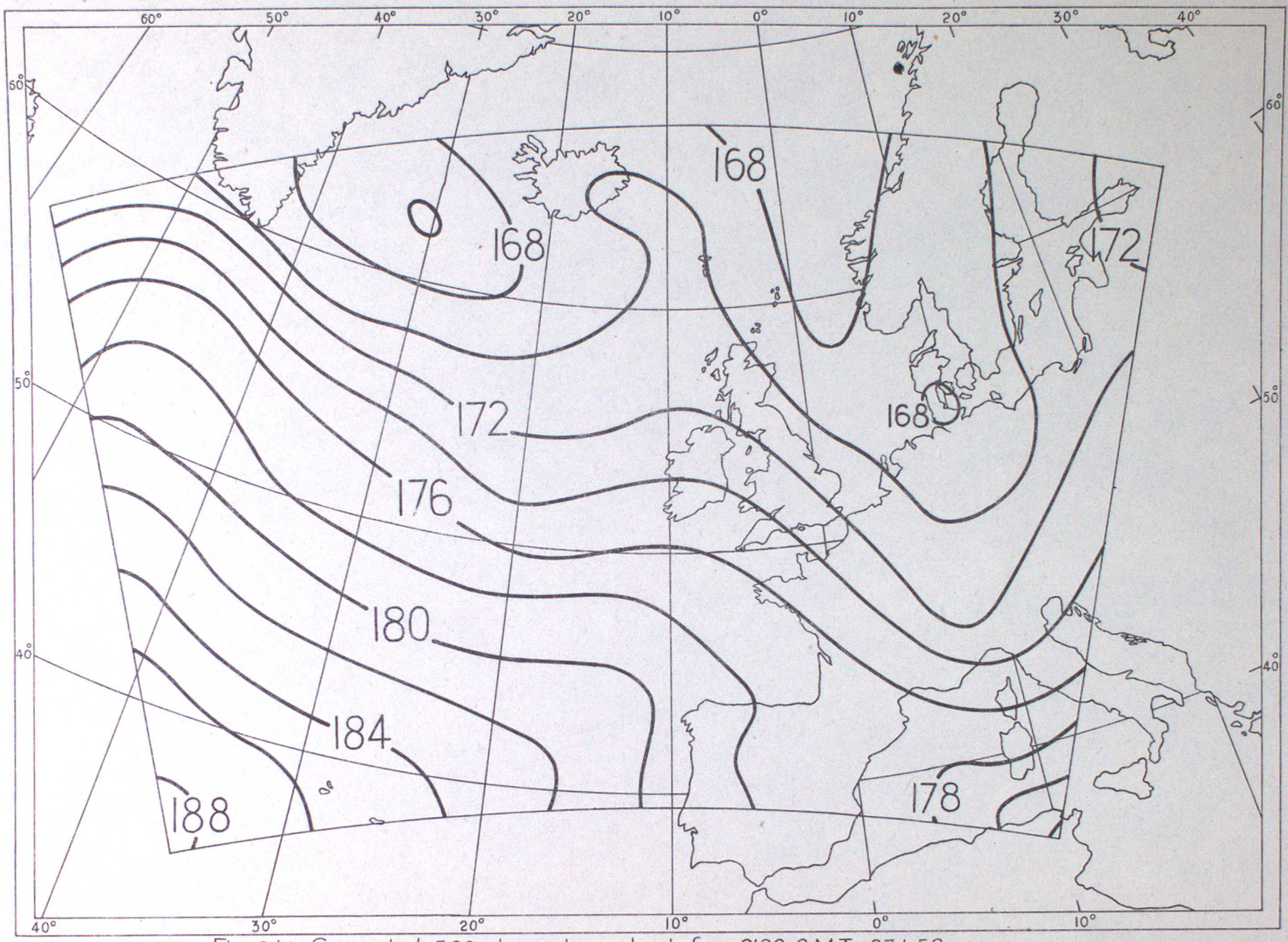

Fig. 2(b) Computed 500mb. contour chart for 2100 G.M.T. 27.1.52

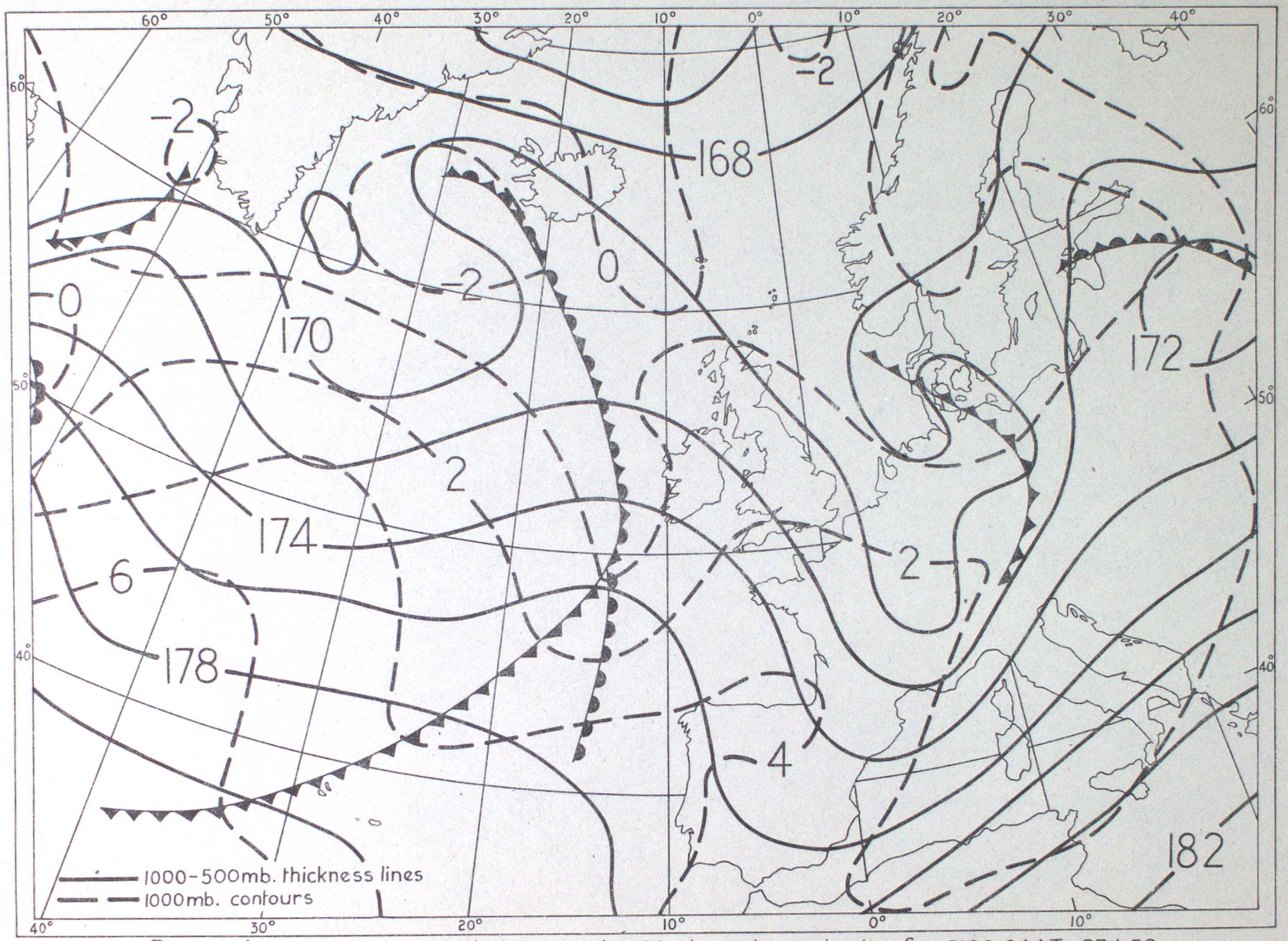

Fig. 2(c) Actual 1000-500mb. thickness and 1000mb. contour charts for 2100 G.M.T. 27.1.52

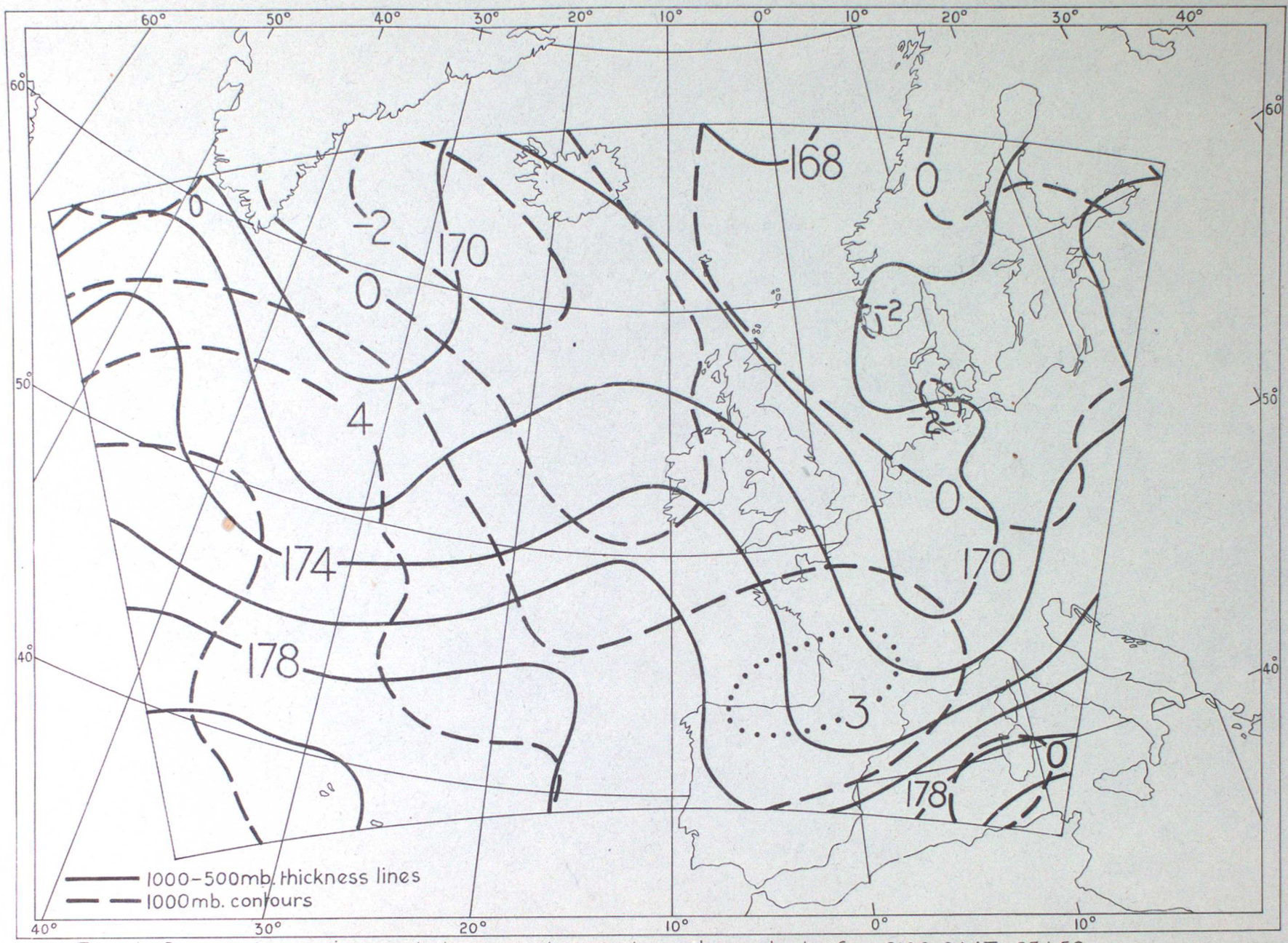

Fig. 2(d) Computed 1000-500mb. thickness and 1000mb. contour charts for 2100 G.M.T. 27.1.52

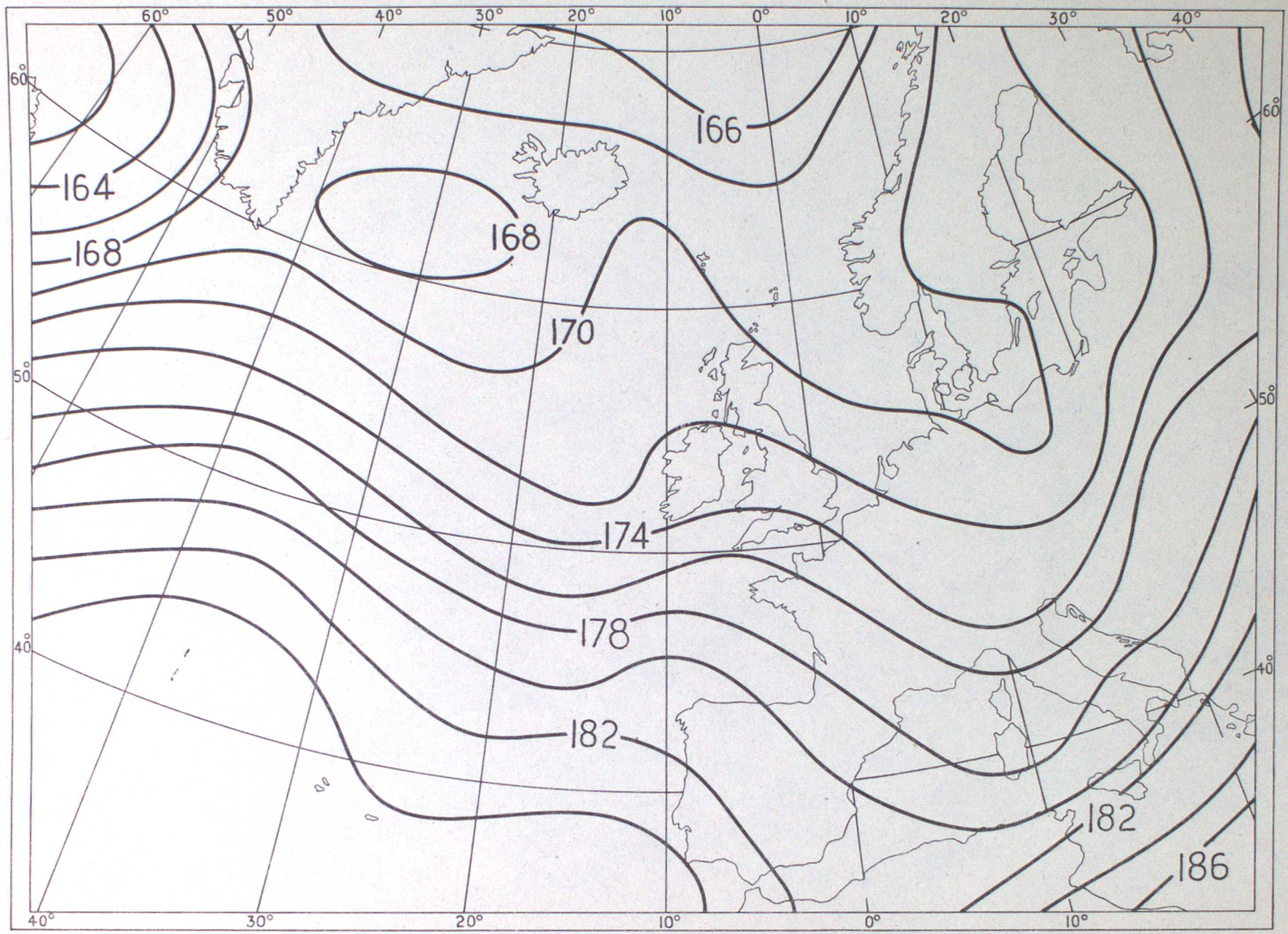

Fig.3(a) Actual 500mb. contours for 0300 G.M.T. 28.1.52

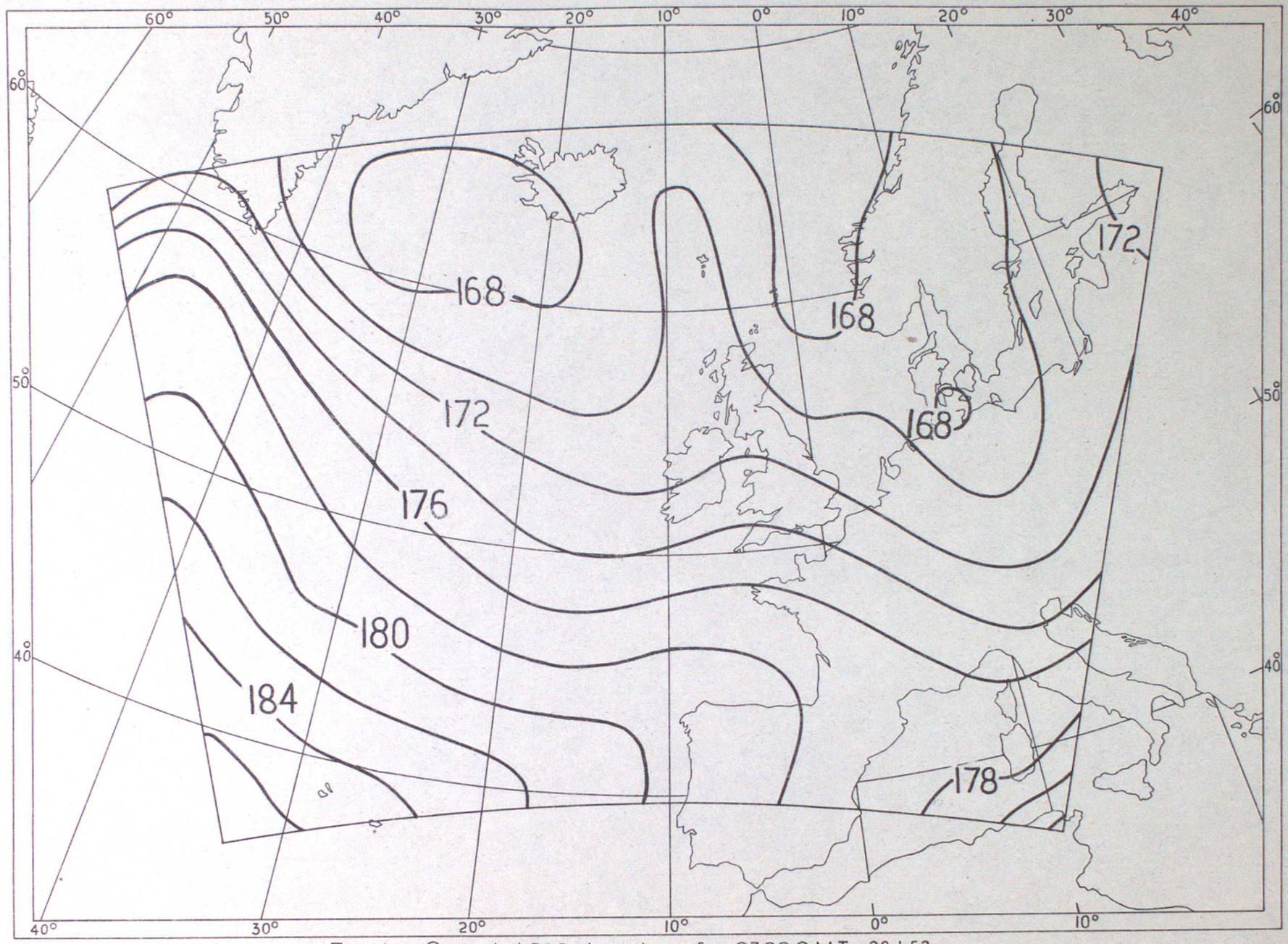

Fig. 3(b) Computed 500mb. contours for 0300 G.M.T. 28.1.52

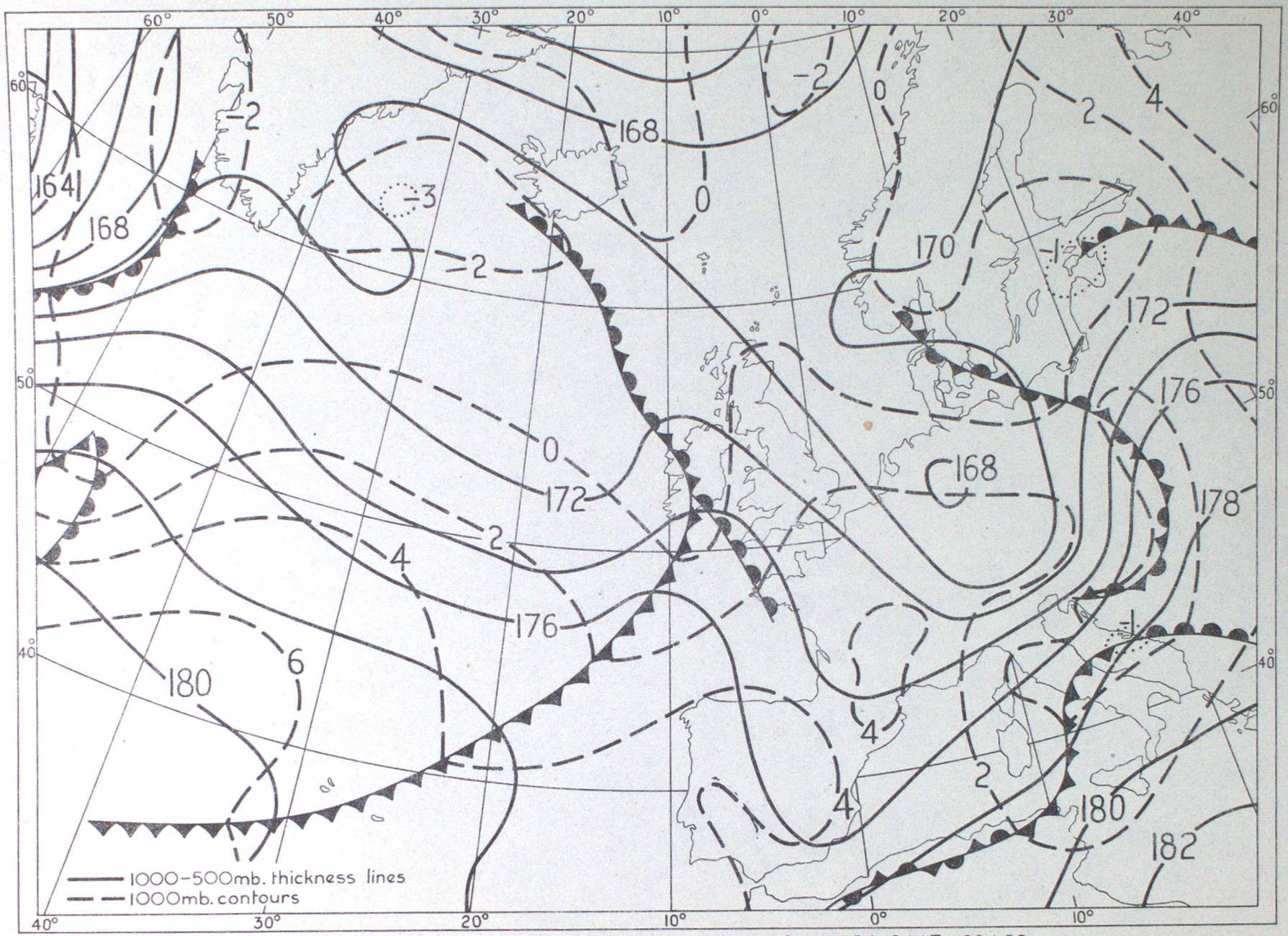

Fig. 3(c) Actual 1000-500mb. thickness and 1000mb. contours for 0300 G.M.T. 28.1.52

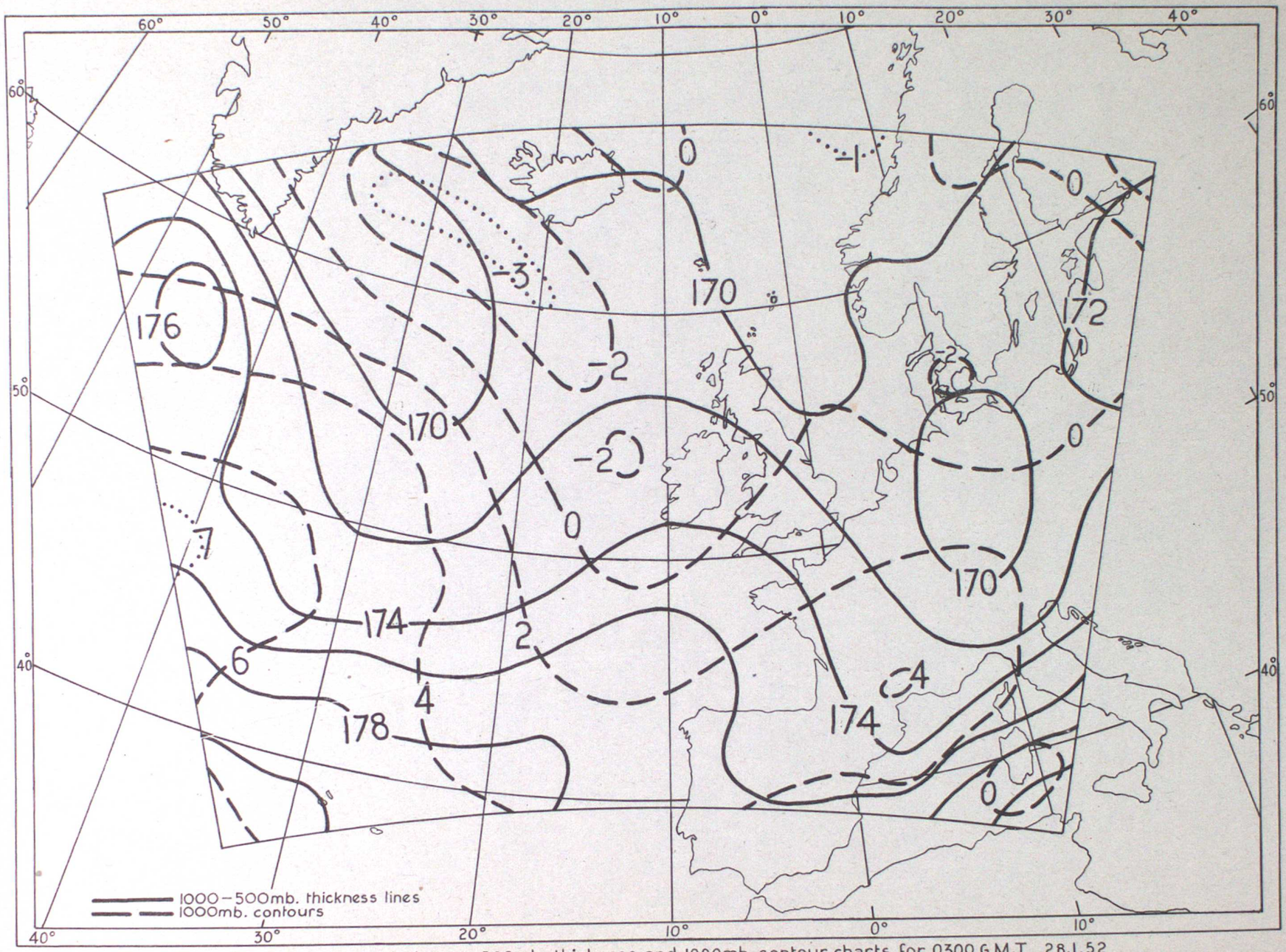

Fig. 3(d) Computed 1000–500mb. thickness and 1000mb. contour charts for 0300 G.M.T. 28.1.52

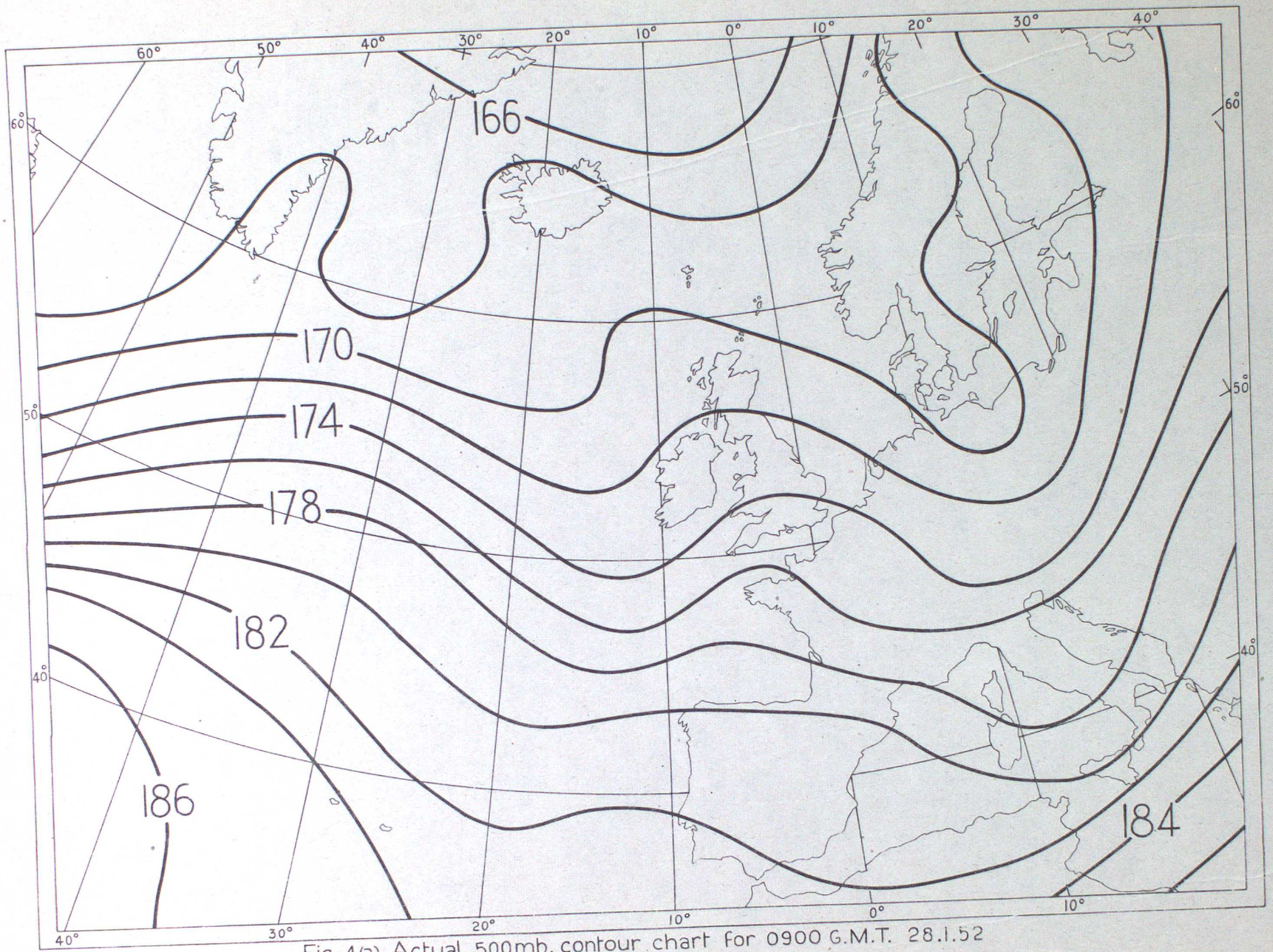

Fig. 4(a) Actual 500mb. contour chart for 0900 G.M.T. 28.1.52

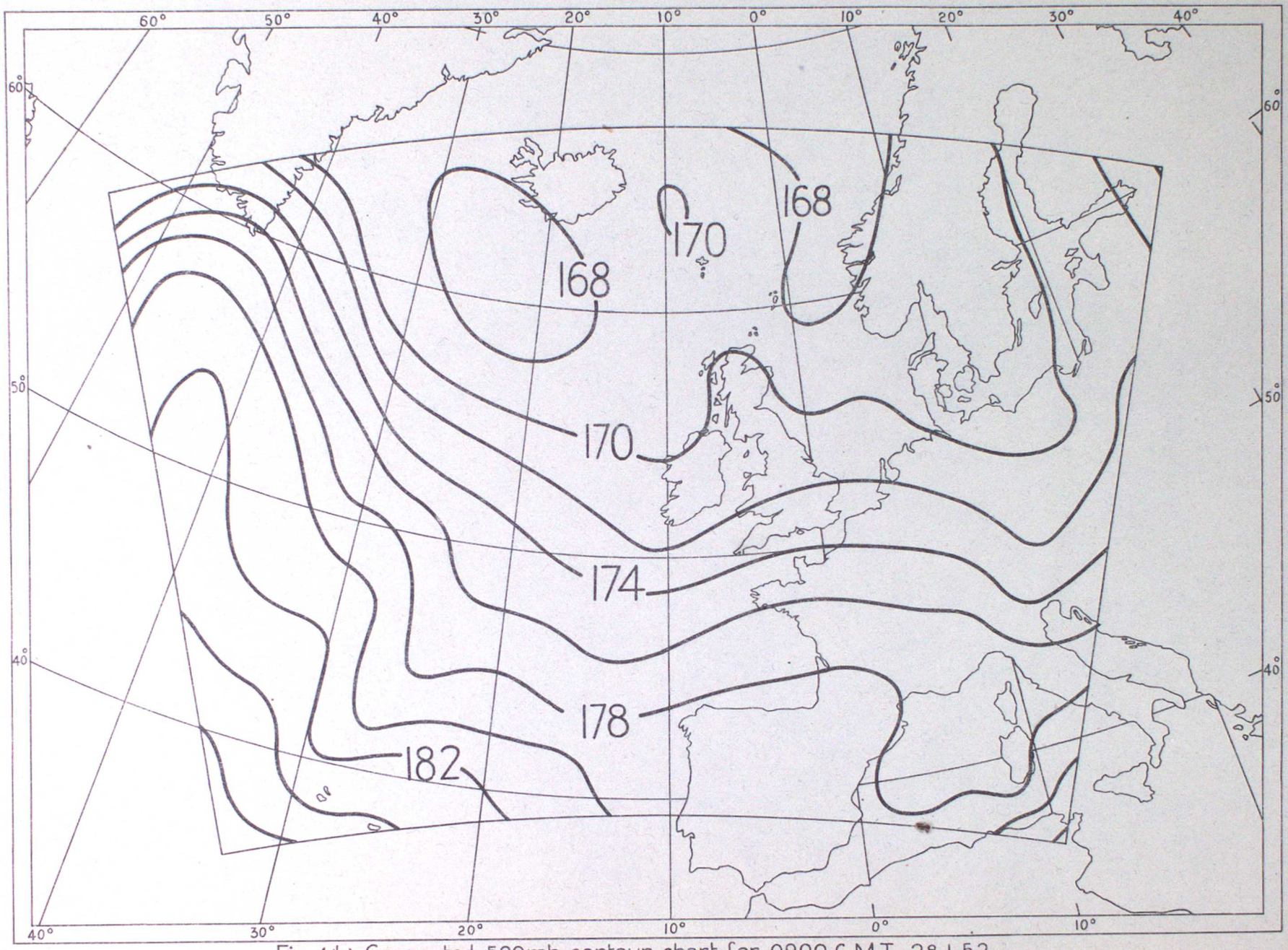

Fig. 4(b) Computed 500mb. contour chart for 0900 G.M.T. 28.1.52

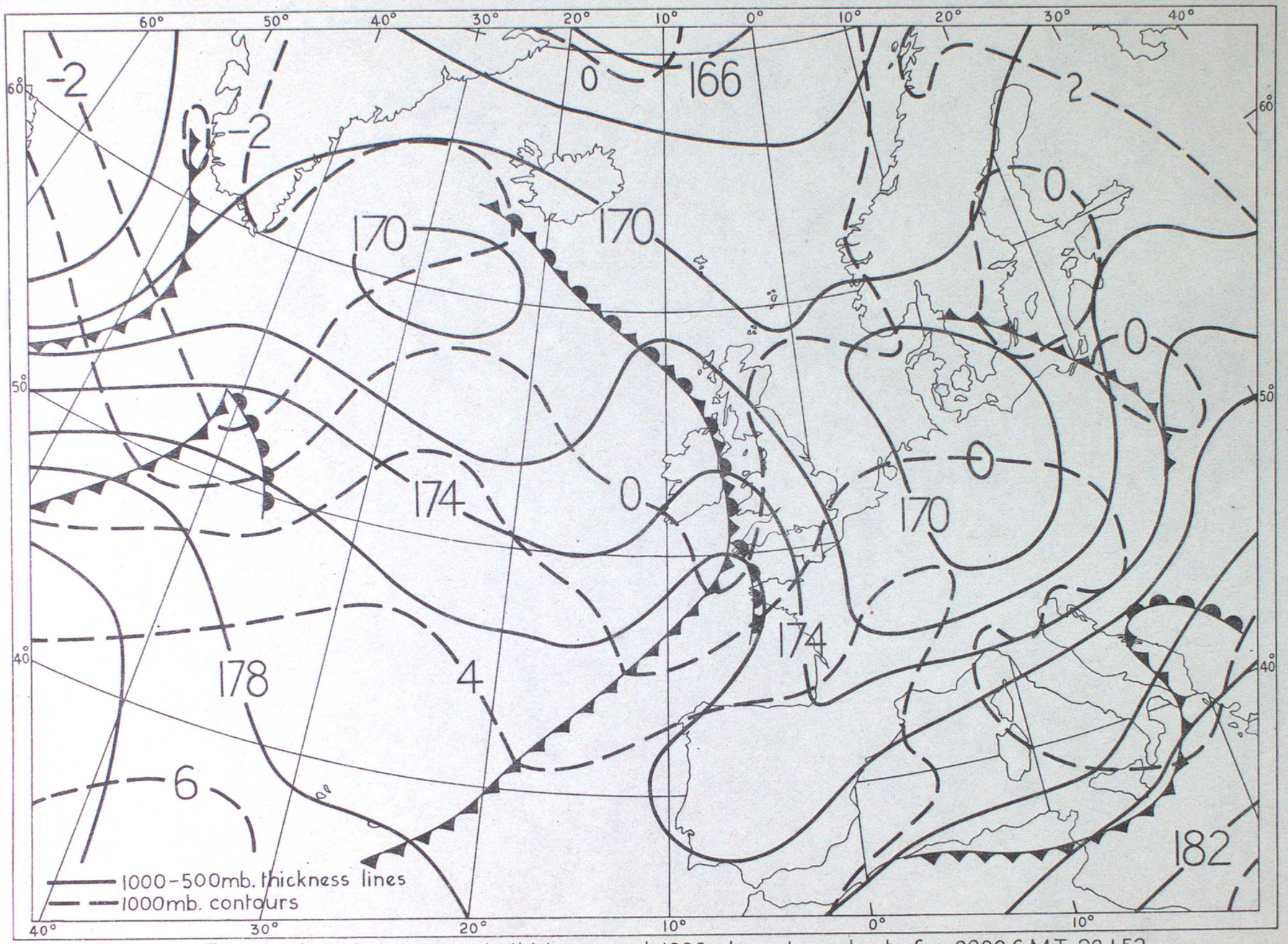

Fig. 4(c) Actual 1000-500mb. thickness and 1000mb. contour charts for 0900 G.M.T. 28.1.52

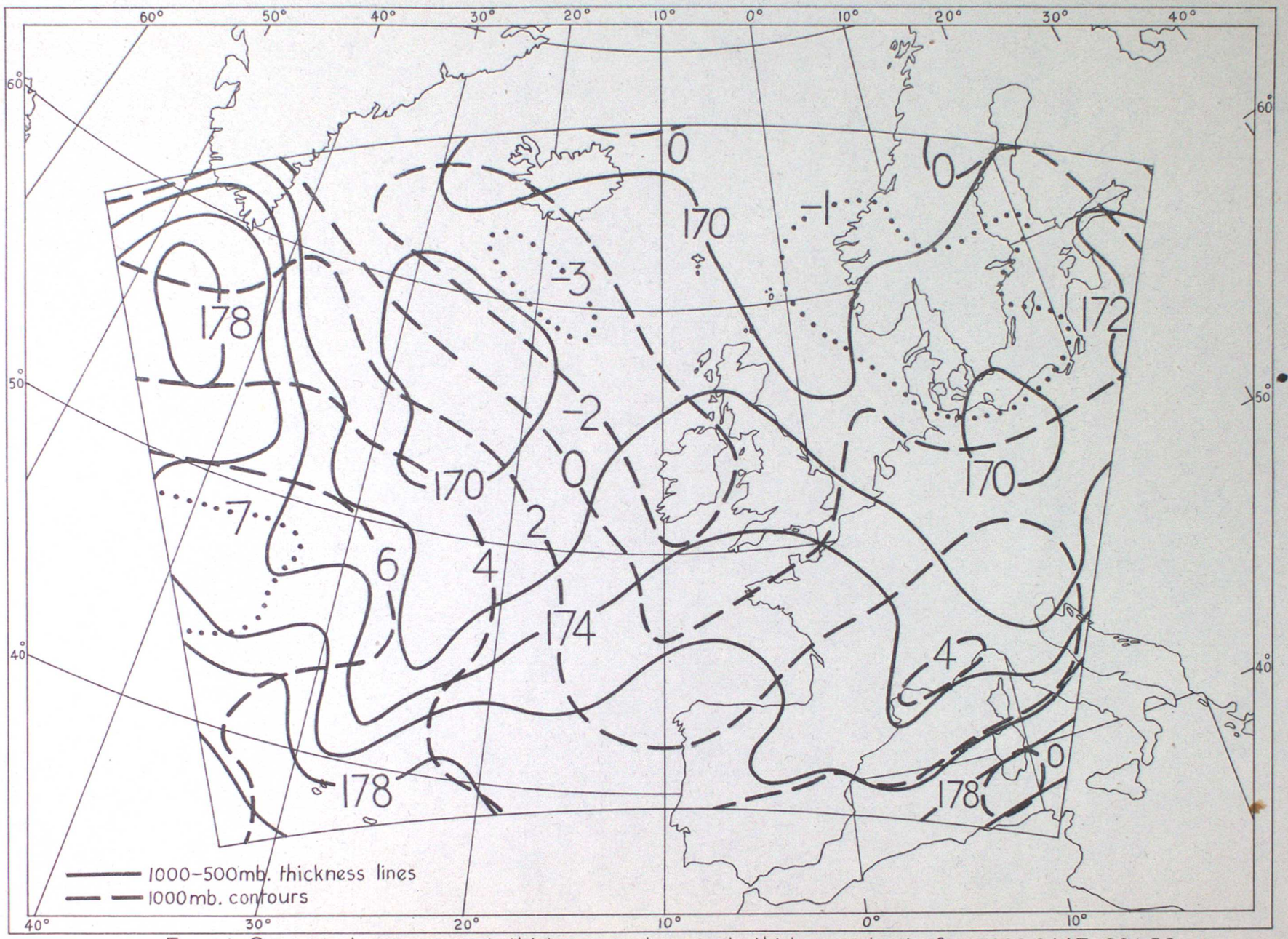

Fig.4(d) Computed 1000–500mb. thickness and 1000mb. thickness charts for 0900 G.M.T. 28.1.52

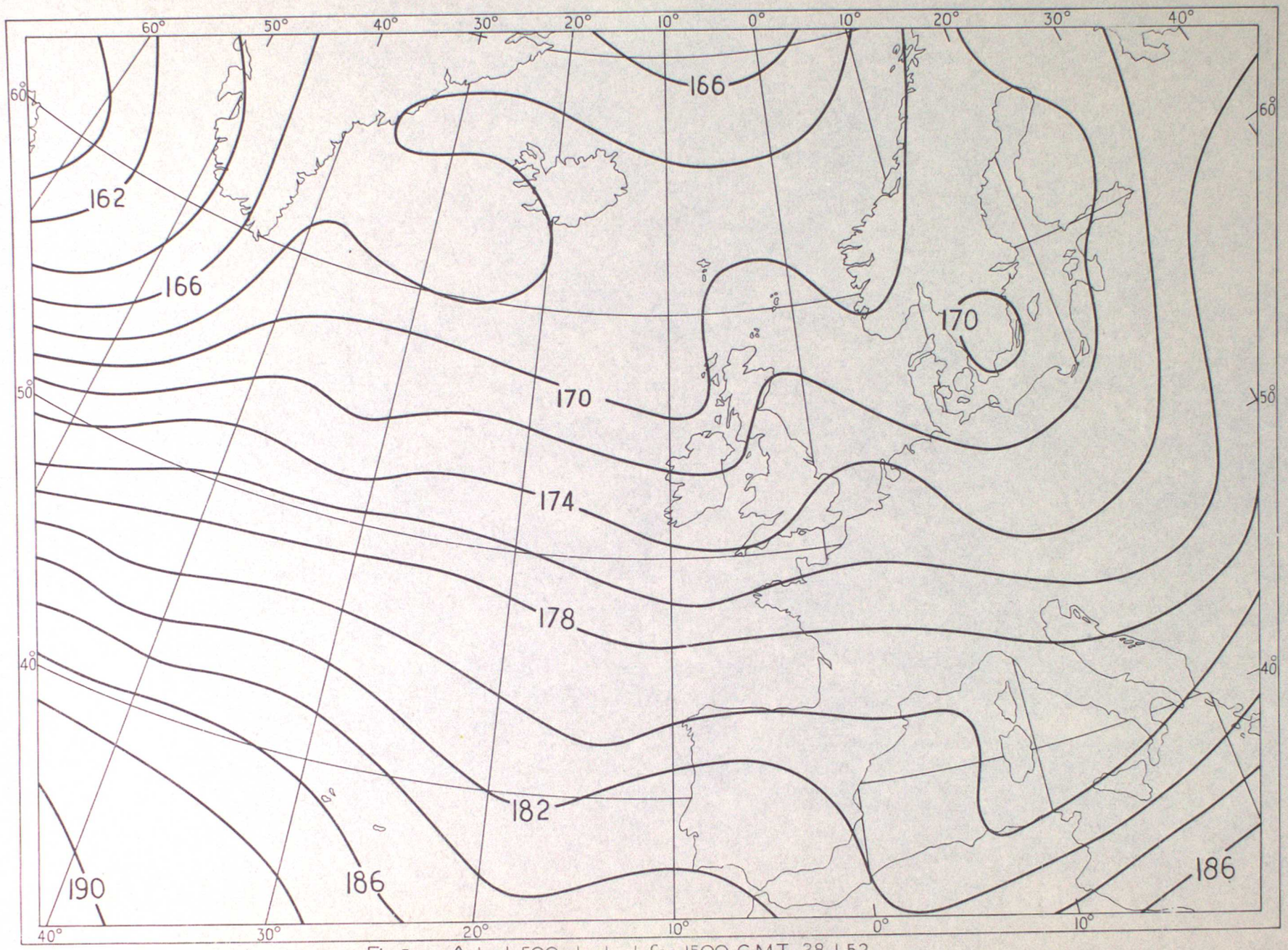

Fig. 5(a) Actual 500mb. chart for 1500 G.M.T. 28.1.52

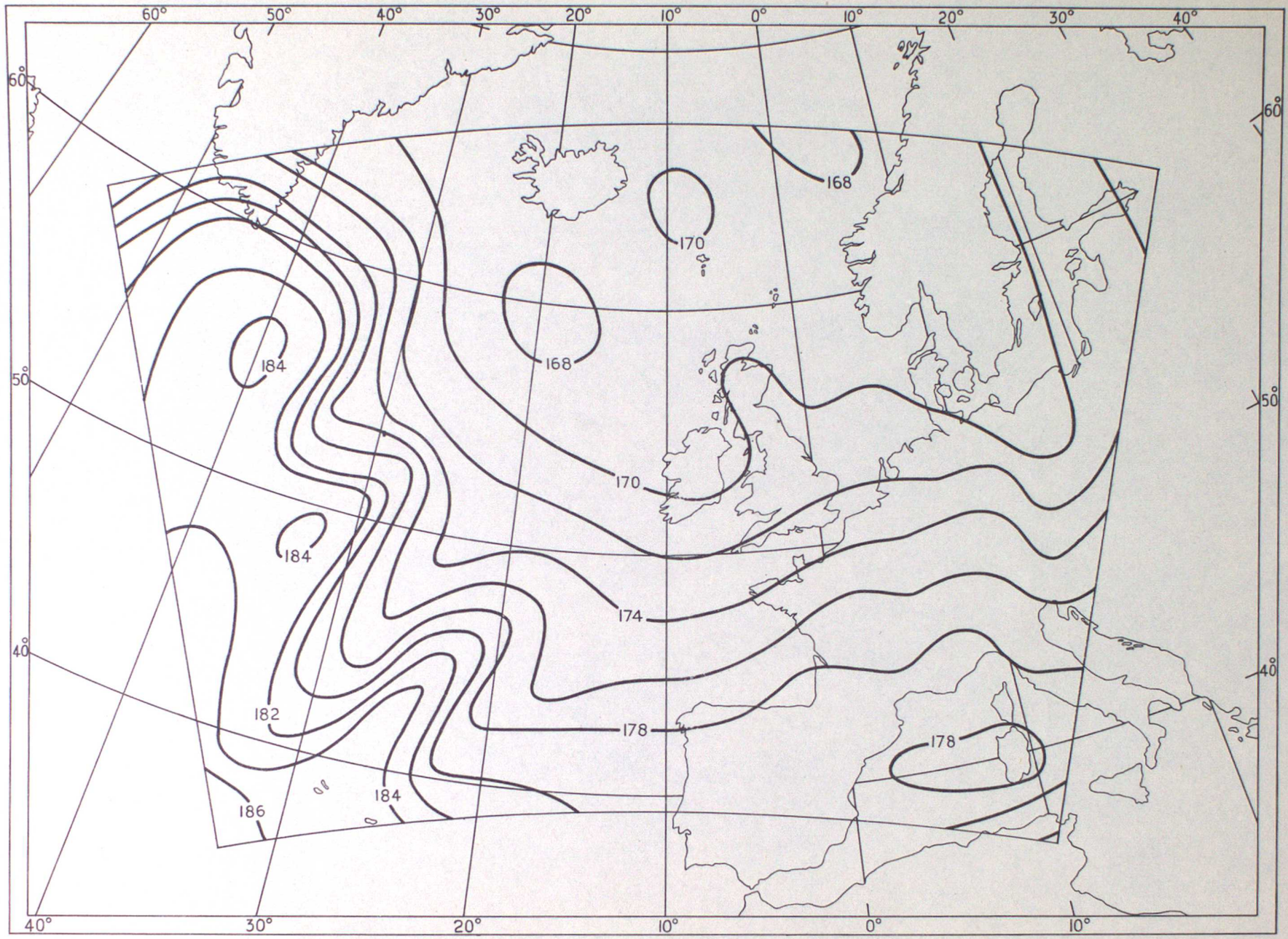

Fig. 5(b) Computed 500mb. chart for 1500 G.M.T. 28.1.52

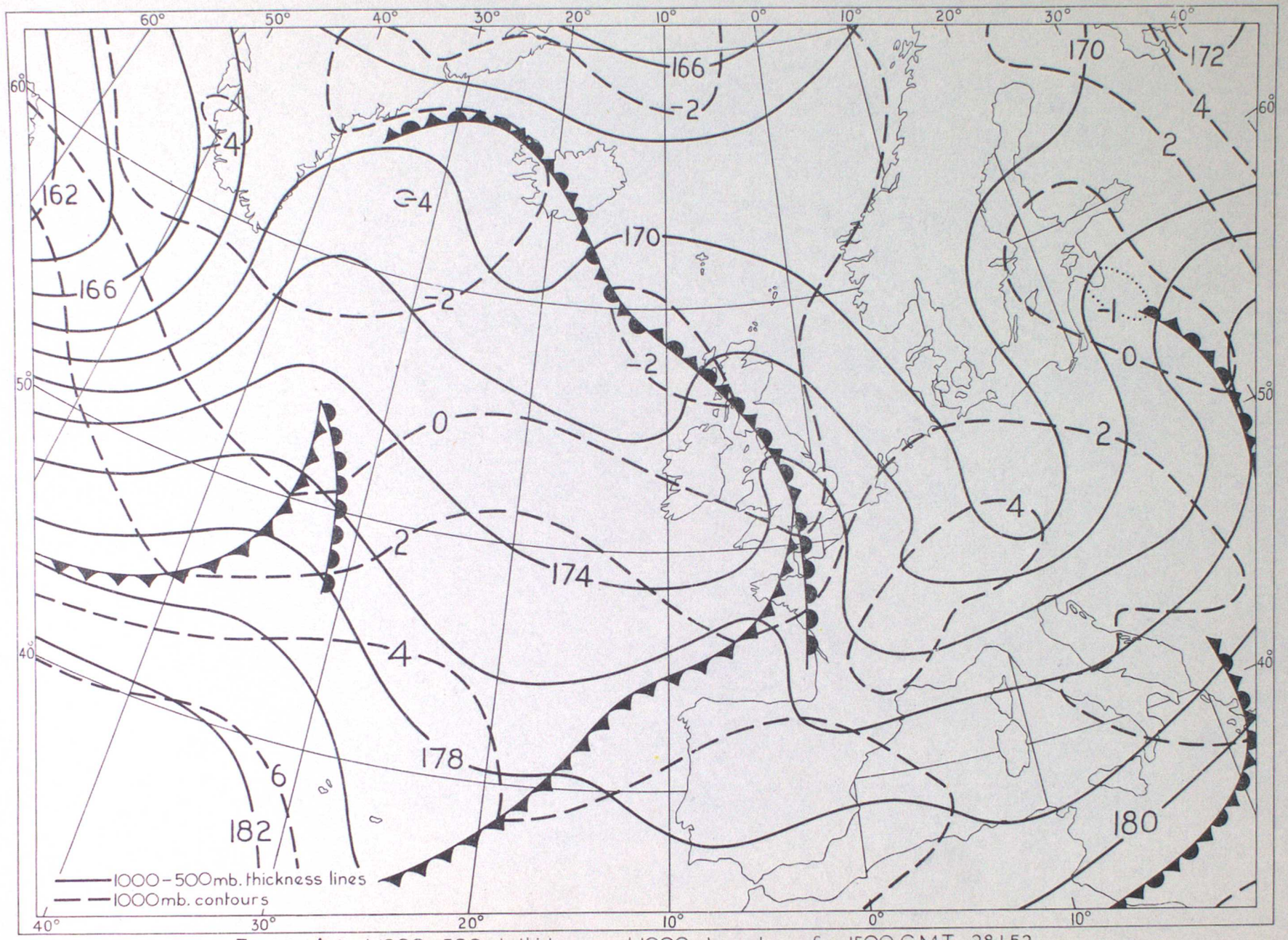

Fig. 5(c) Actual 1000-500mb. thickness and 1000mb. contours for 1500 G.M.T. 28.1.52

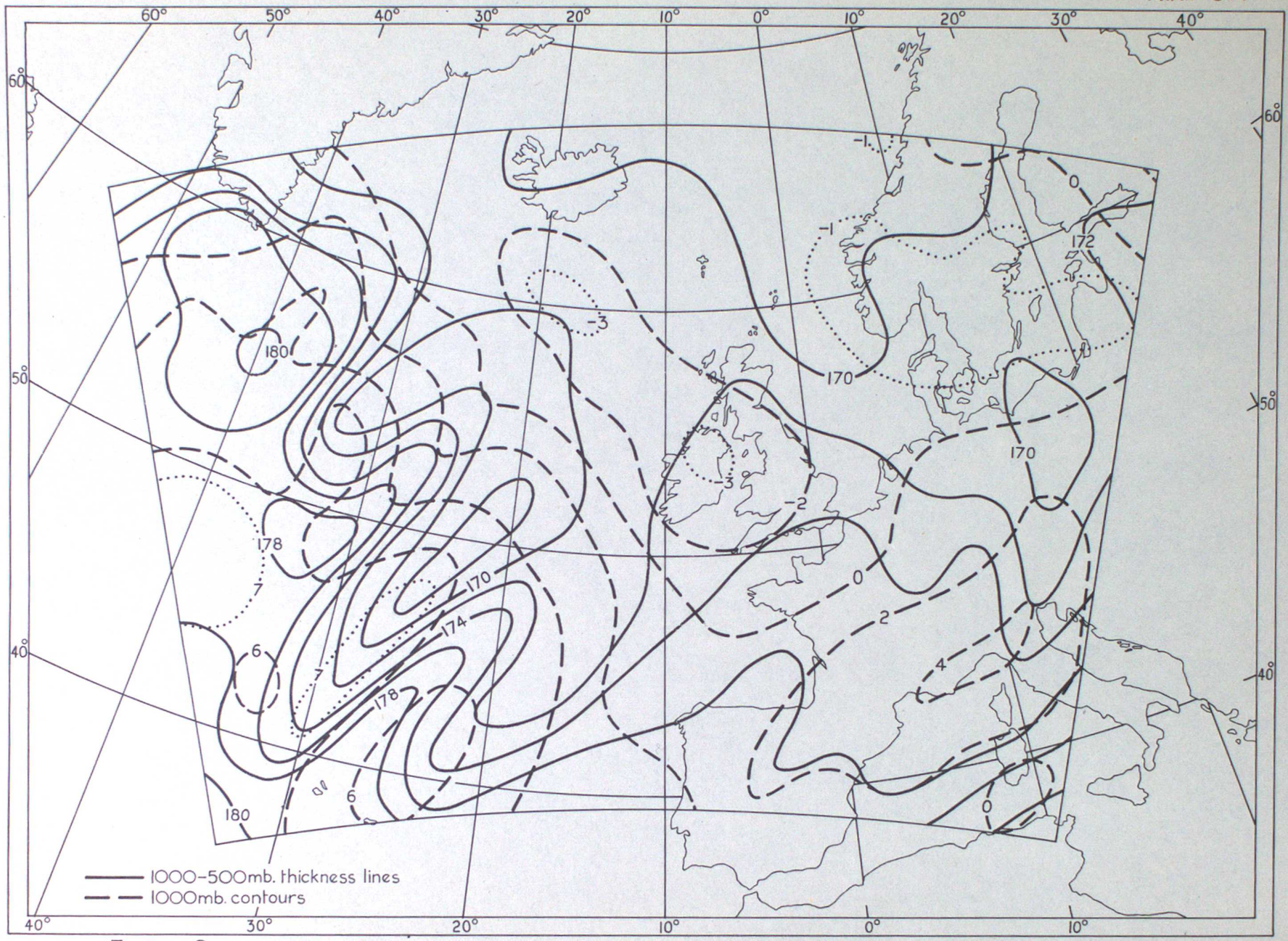

Fig. 5(d) Computed 1000–500mb. thickness and 1000mb. contour charts for 1500 G.M.T. 28.1.52

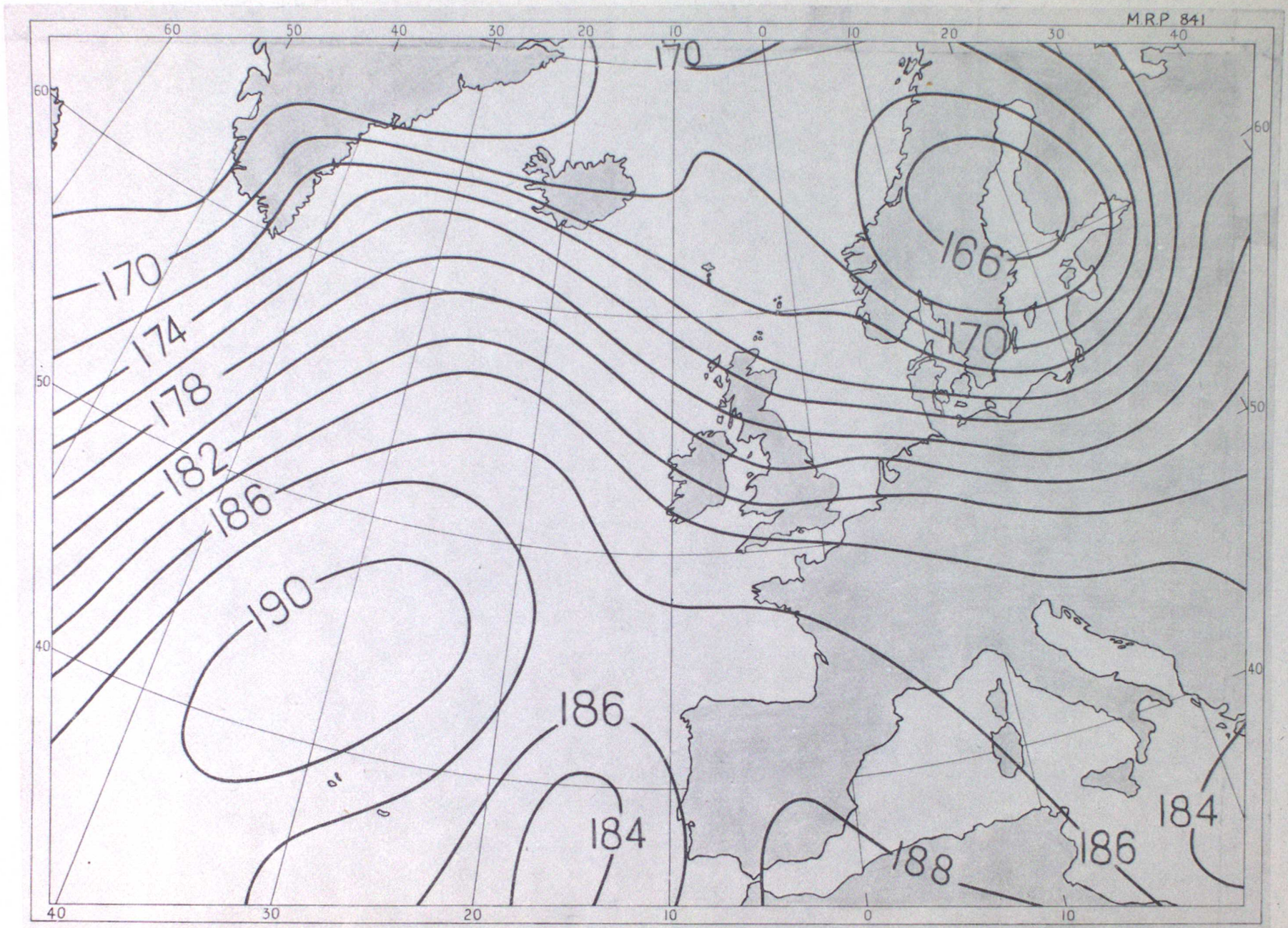

Fig. 6(a) Actual 500mb. contour chart for 1500 G.M.T. 14.3.49

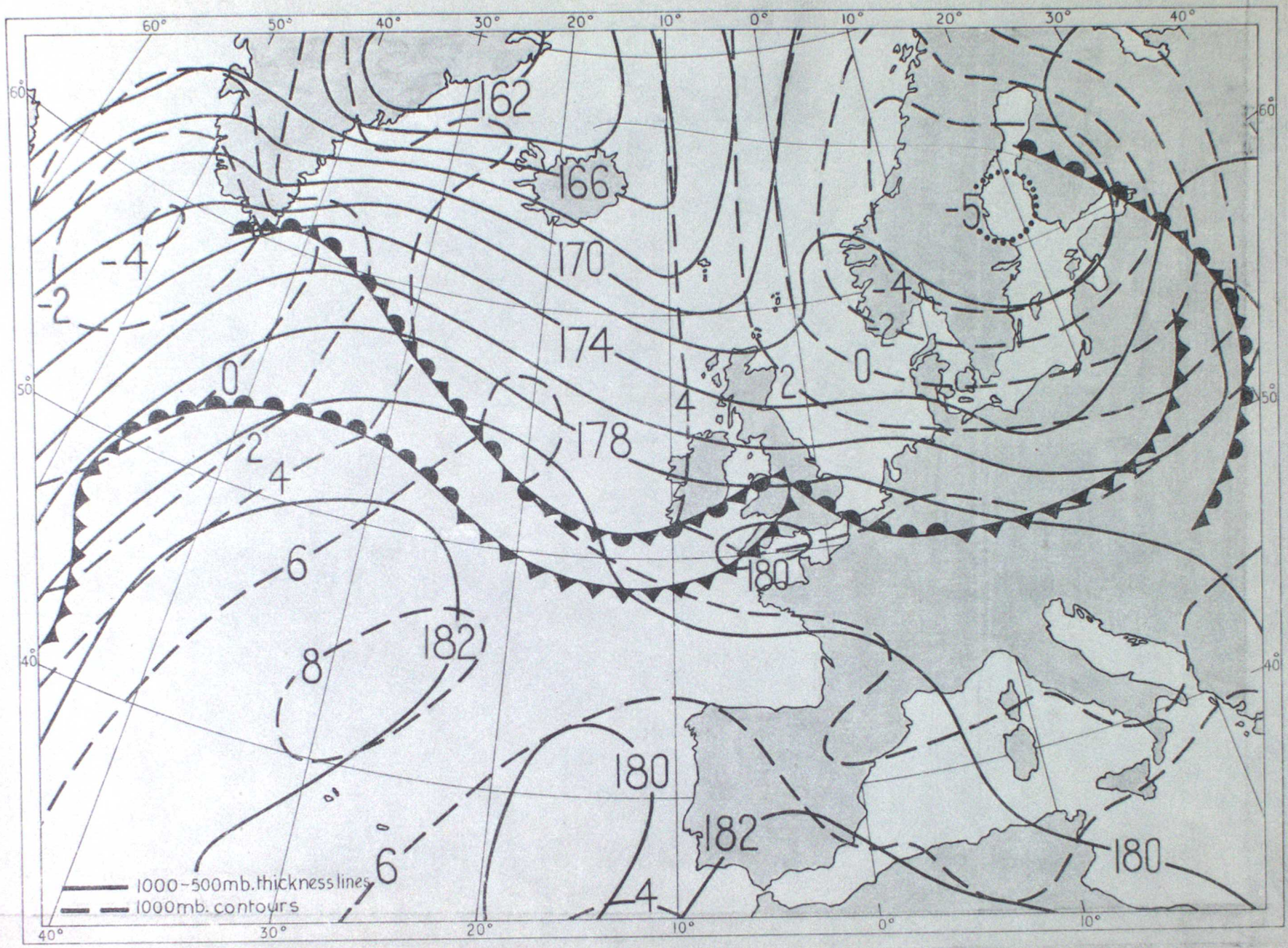

Fig. 6(b) Actual 1000-500mb. thickness and 1000mb. contour charts for 1500 G.M.T. 14.3.49

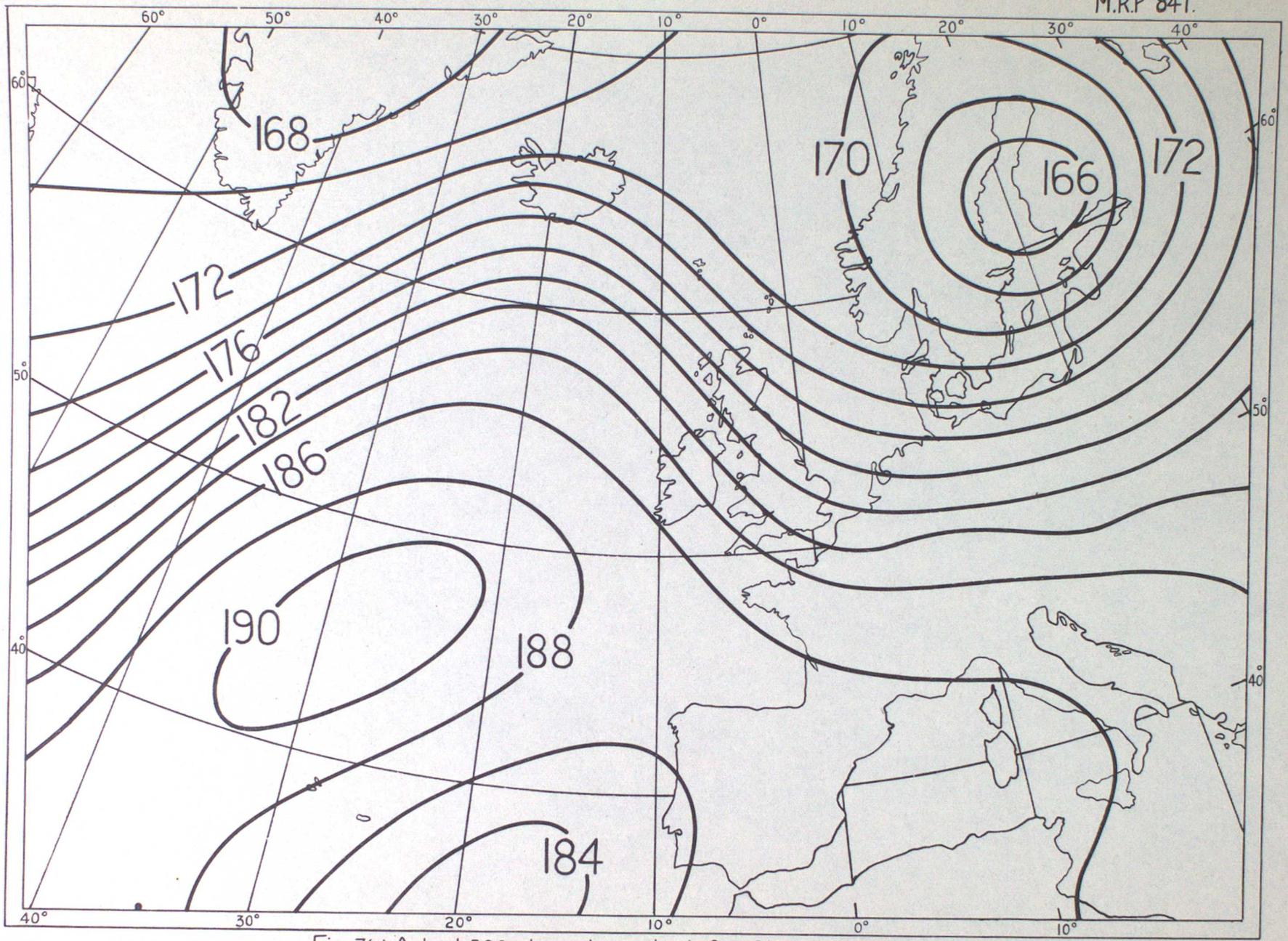

Fig. 7(a) Actual 500mb. contour chart for 2100 G.M.T. 14.3.49

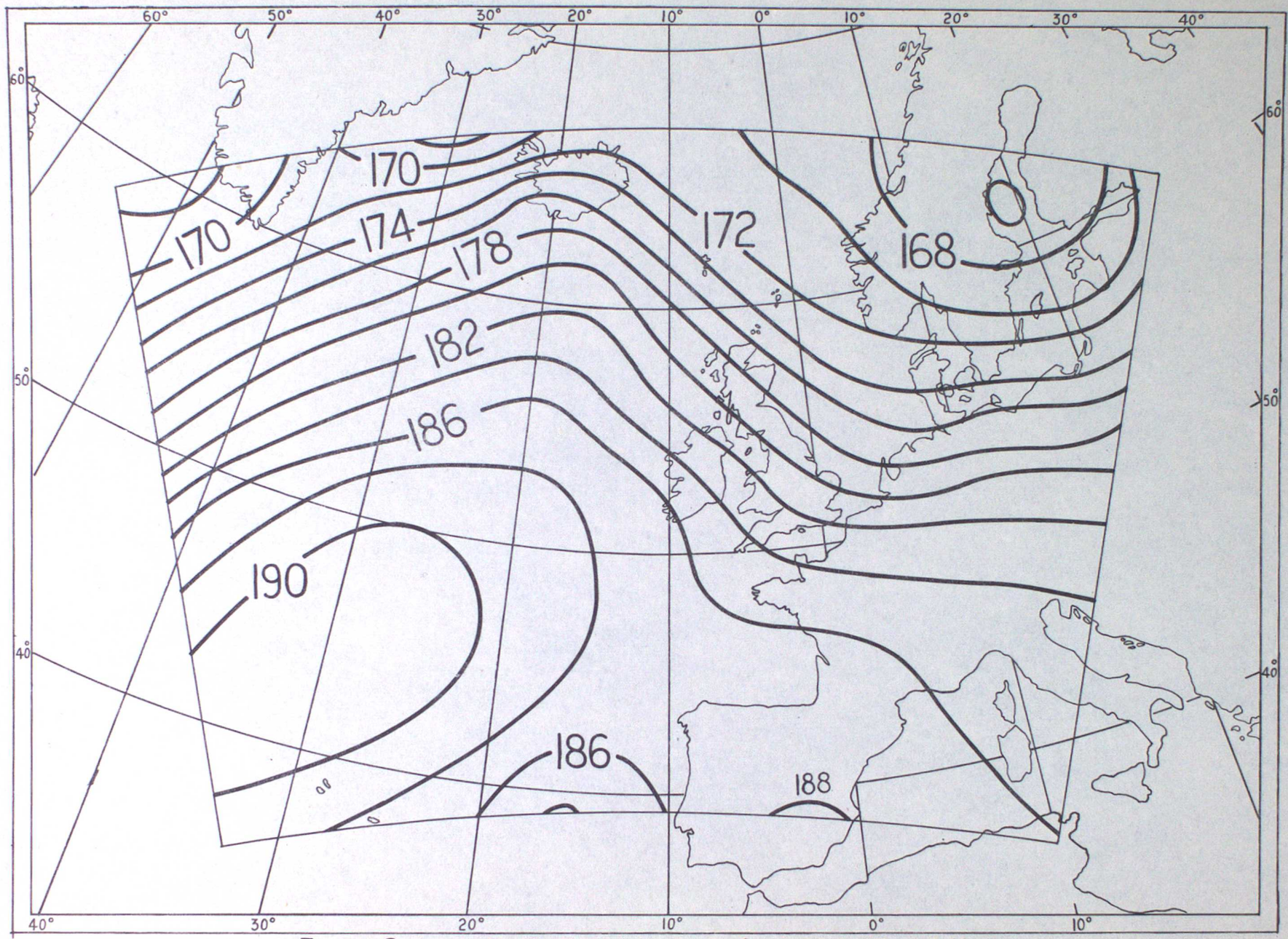

Fig. 7(b) Computed 500mb. contour chart for 2100 G.M.T. 14.3.49

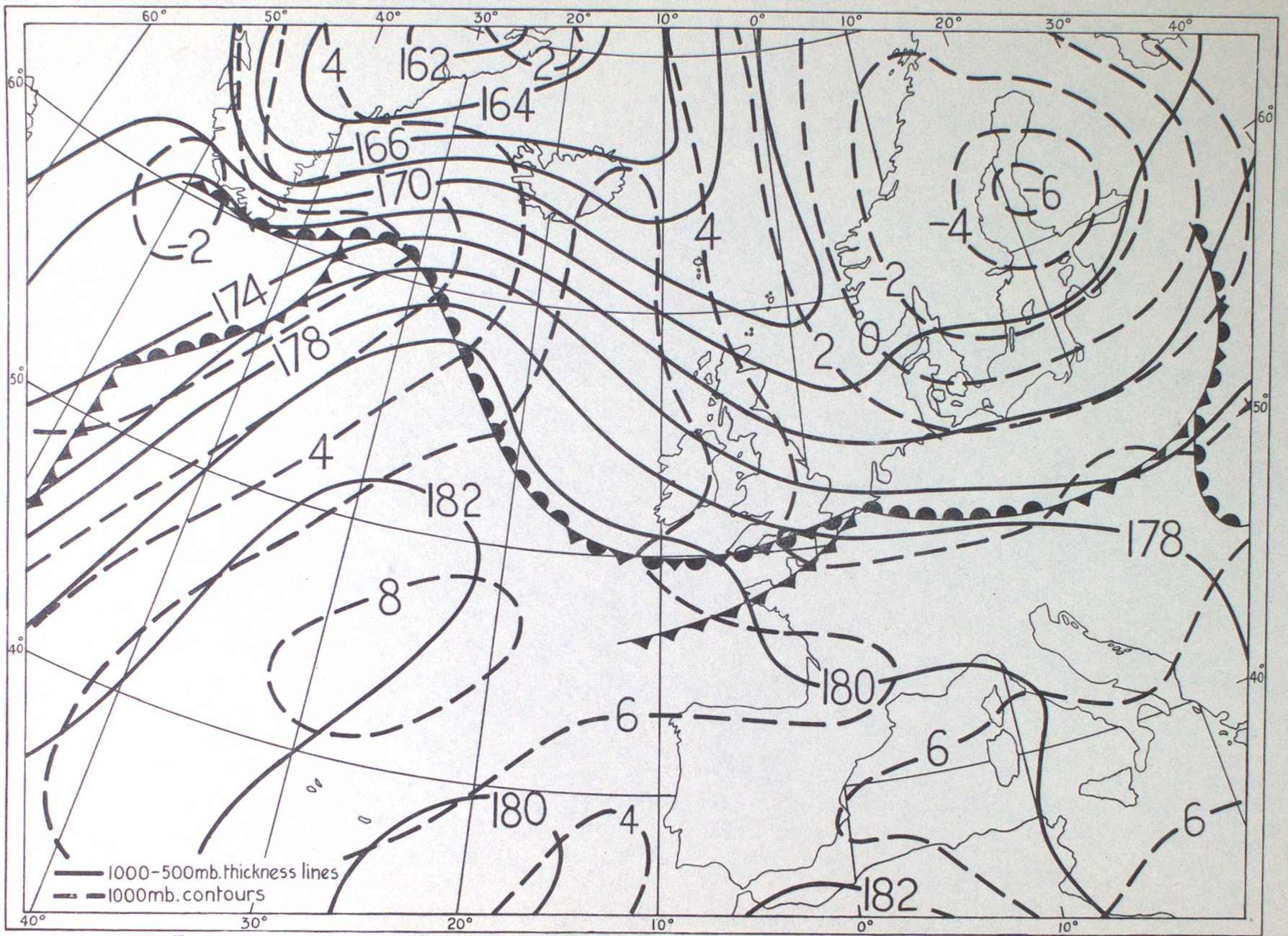

Fig. 7(c) Actual 1000-500mb. thickness and 1000mb. contour charts for 2100 G.M.T. 14.3.49

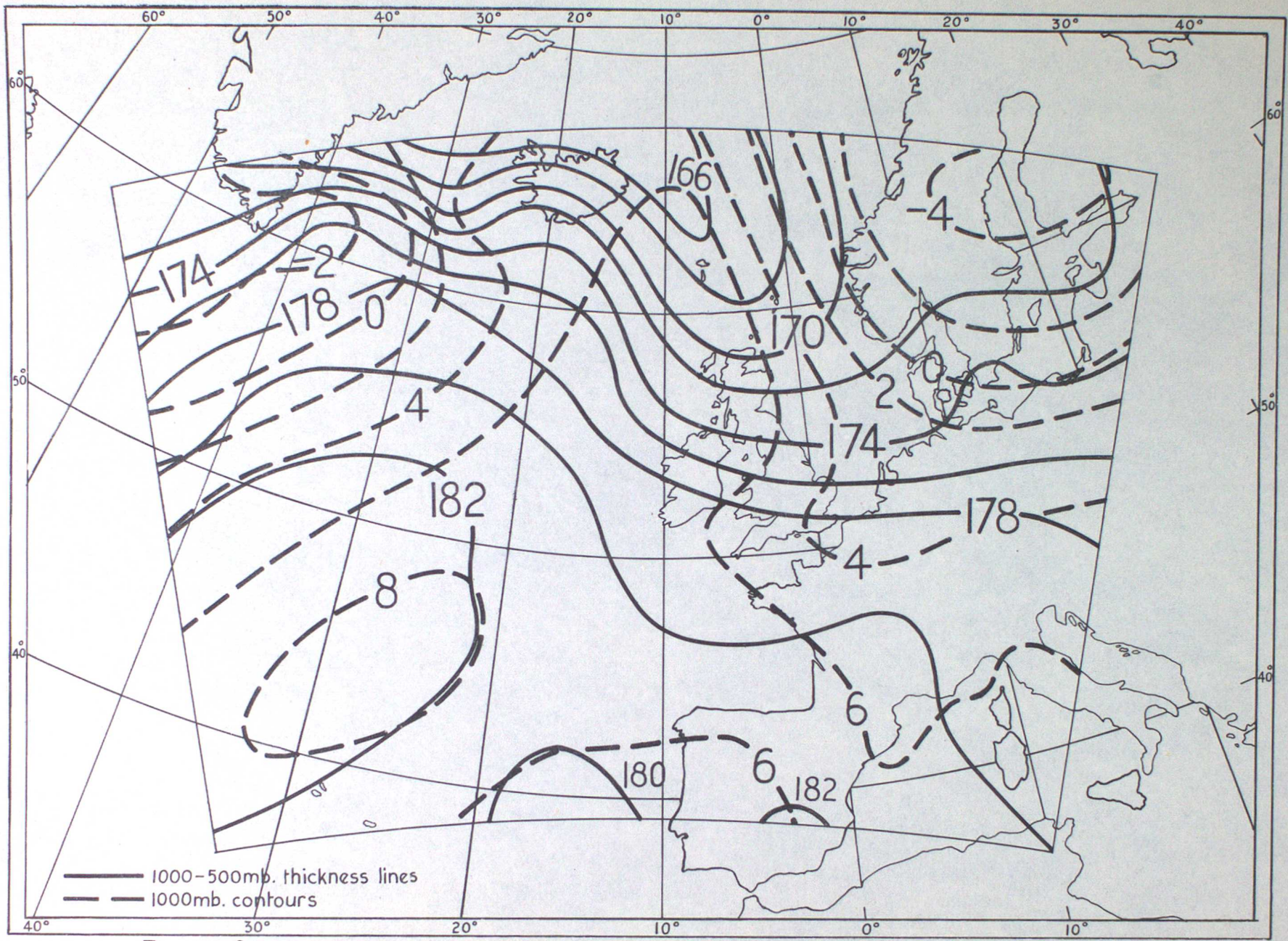

Fig. 7(d) Computed 1000-500mb. thickness and 1000mb. contour charts for 2100 G.M.T. 14.3.49

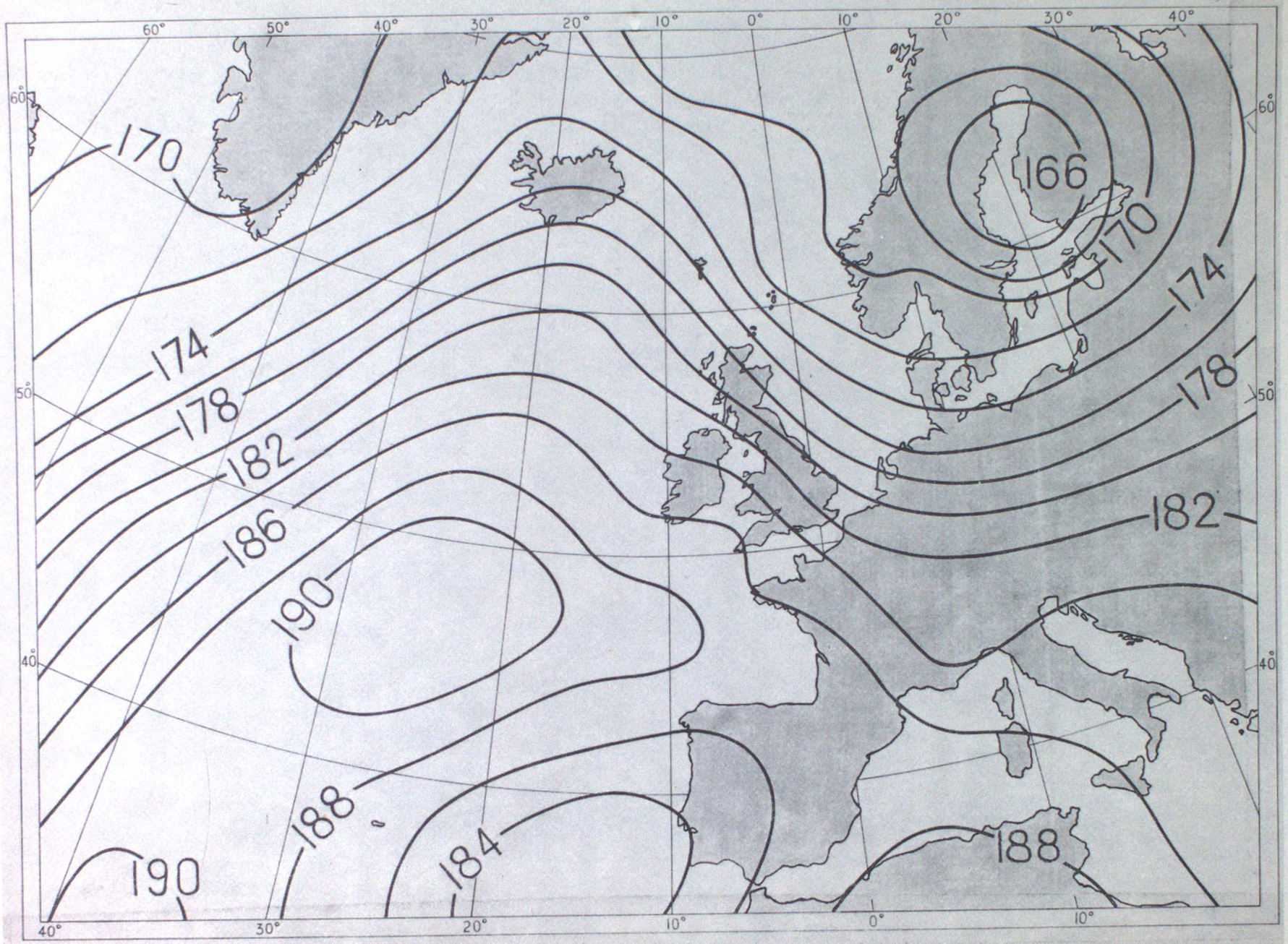

Fig. 8(a) Actual 500mb. contour chart for 0300 G.M.T. 15.3.49

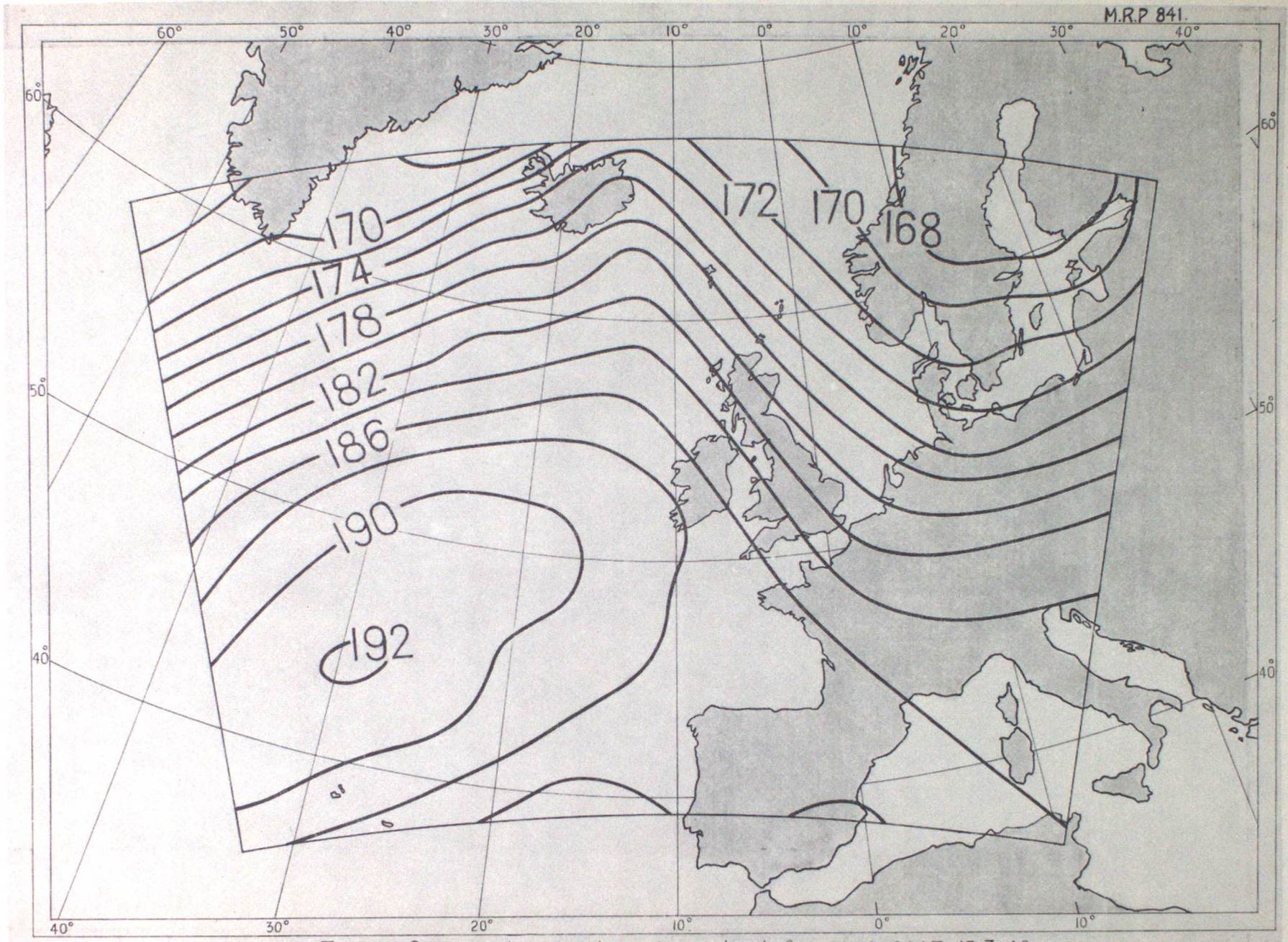

Fig. 8(b) Computed 500mb. contour chart for 0300 G.M.T. 15.3.49

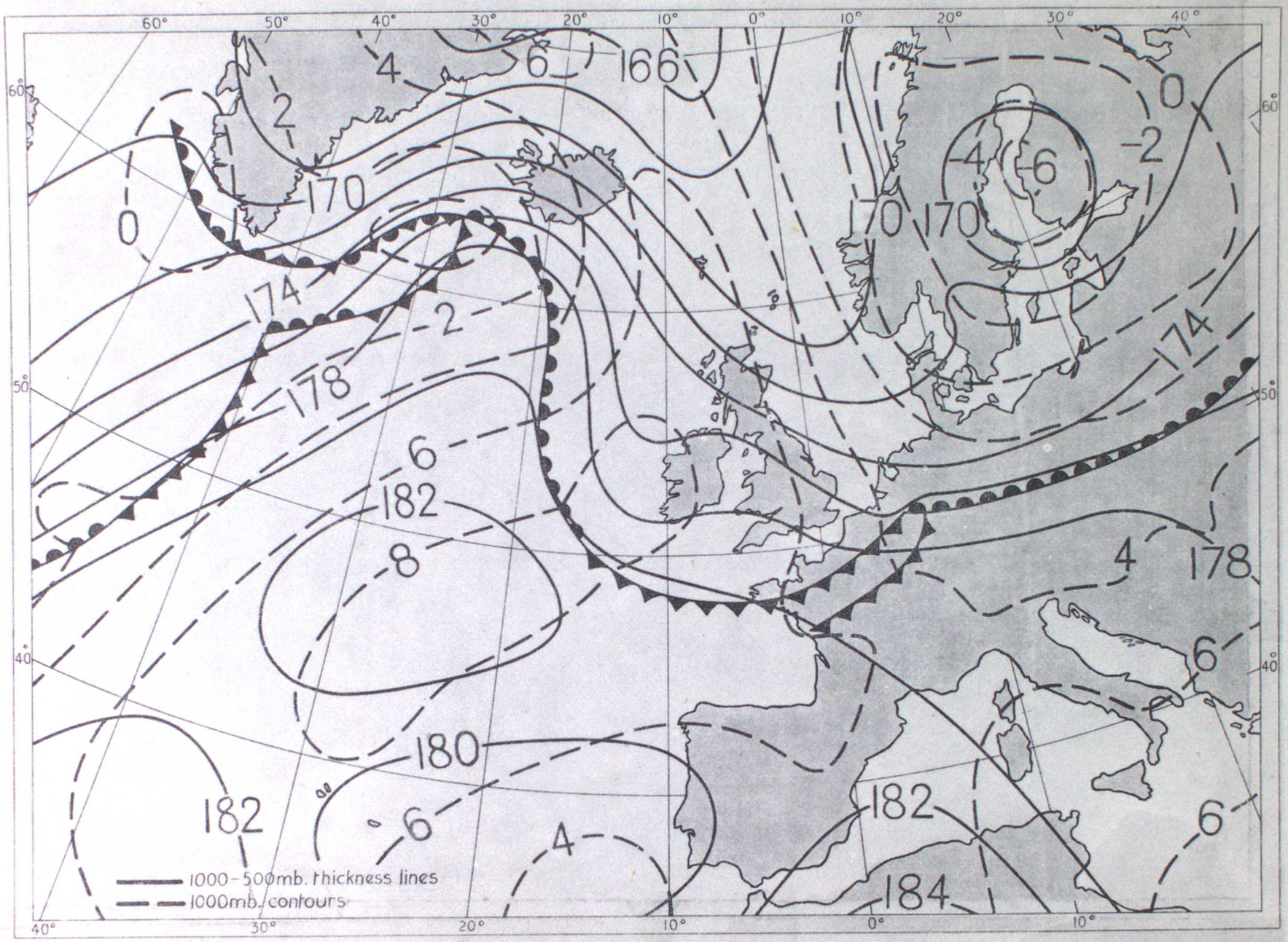

Fig. 8(c) Actual 1000-500mb. thickness and 1000mb. contour charts for 0300 G.M.T. 15.3.49

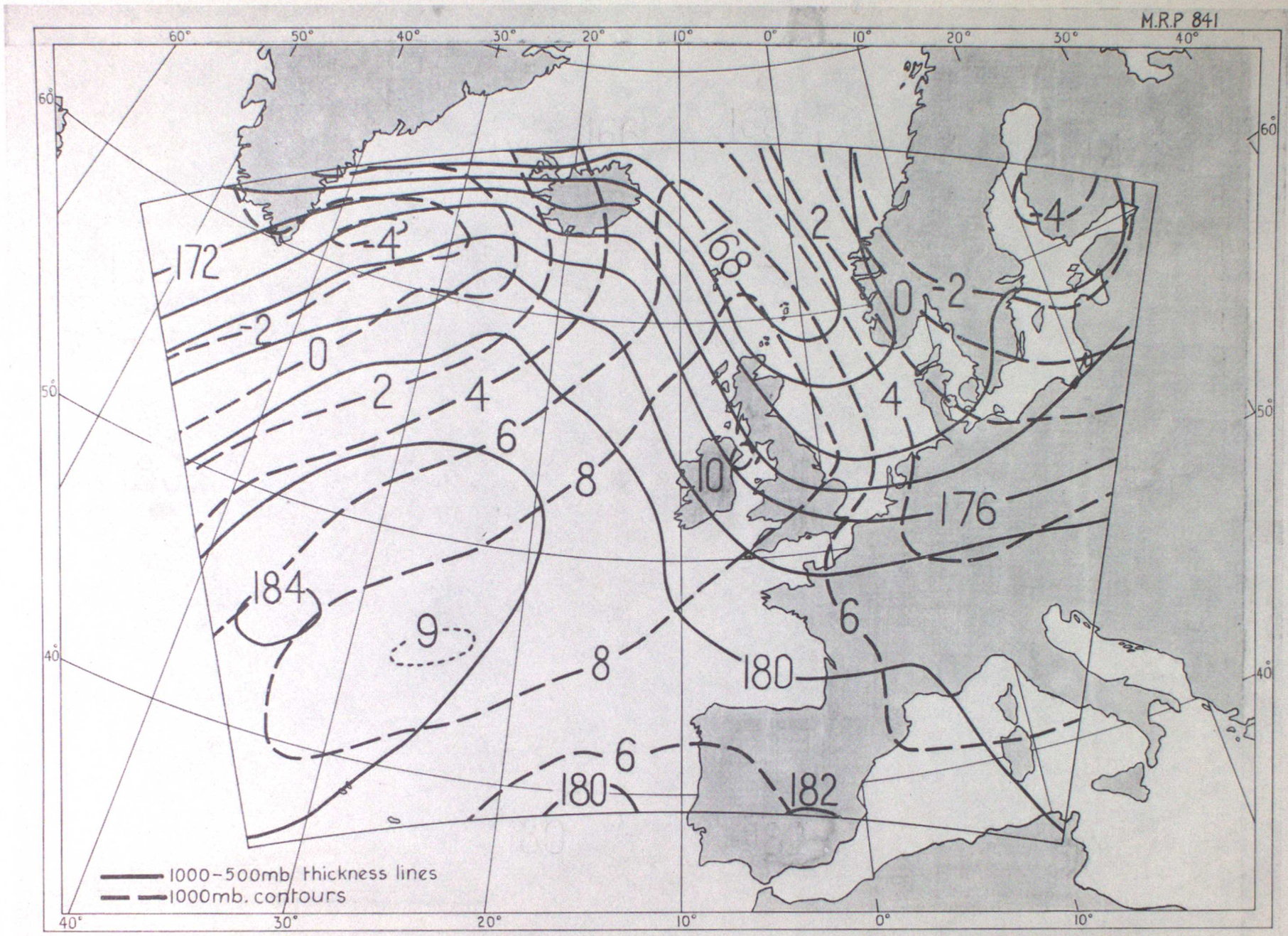

Fig. 8(d) Computed 1000-500mb. thickness and 1000mb. contour charts for 0300 G.M.T. 15.3.49

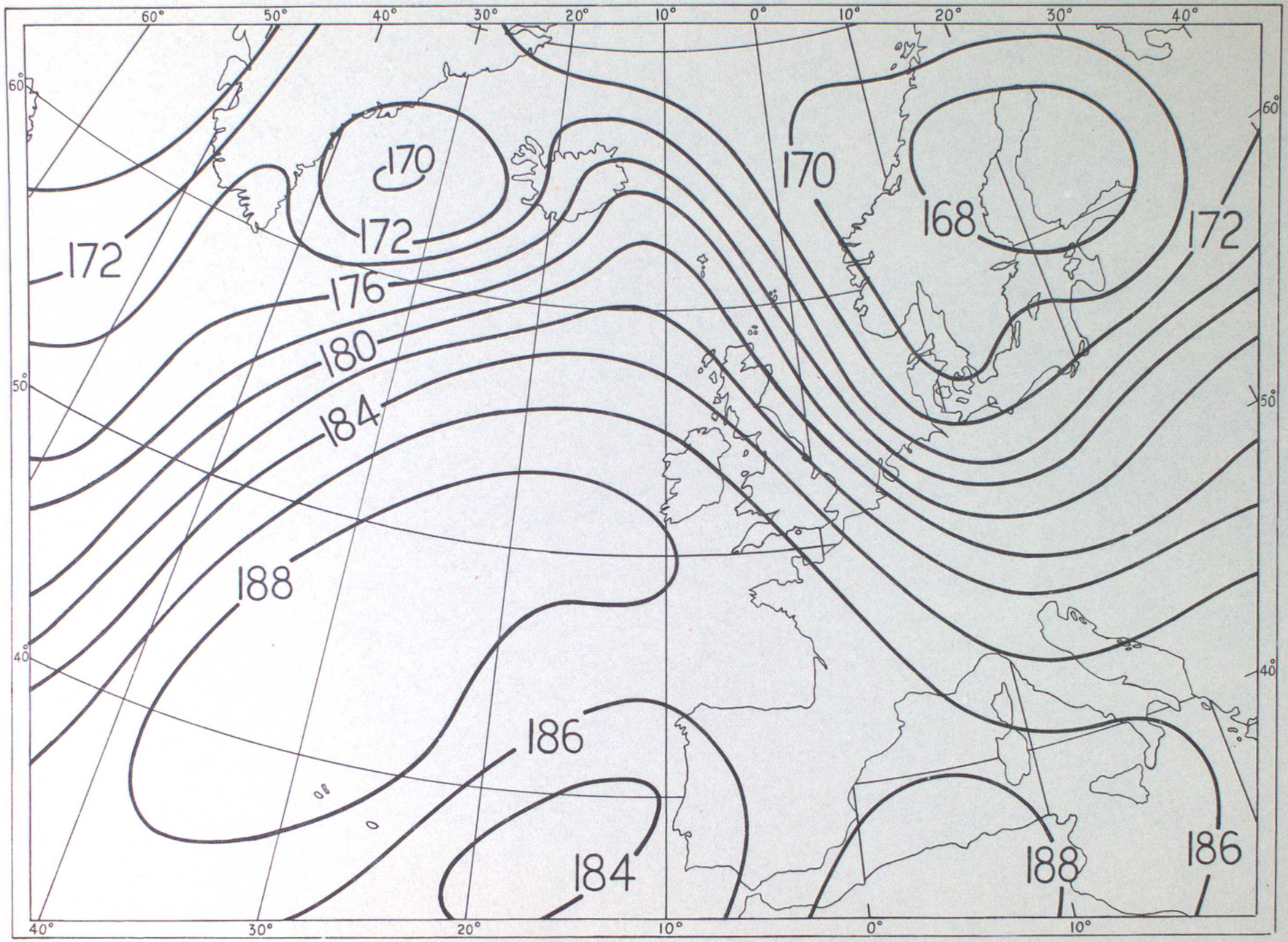

Fig.9(a) Actual 500mb. contour chart for 0900 G.M.T. 15.3.49

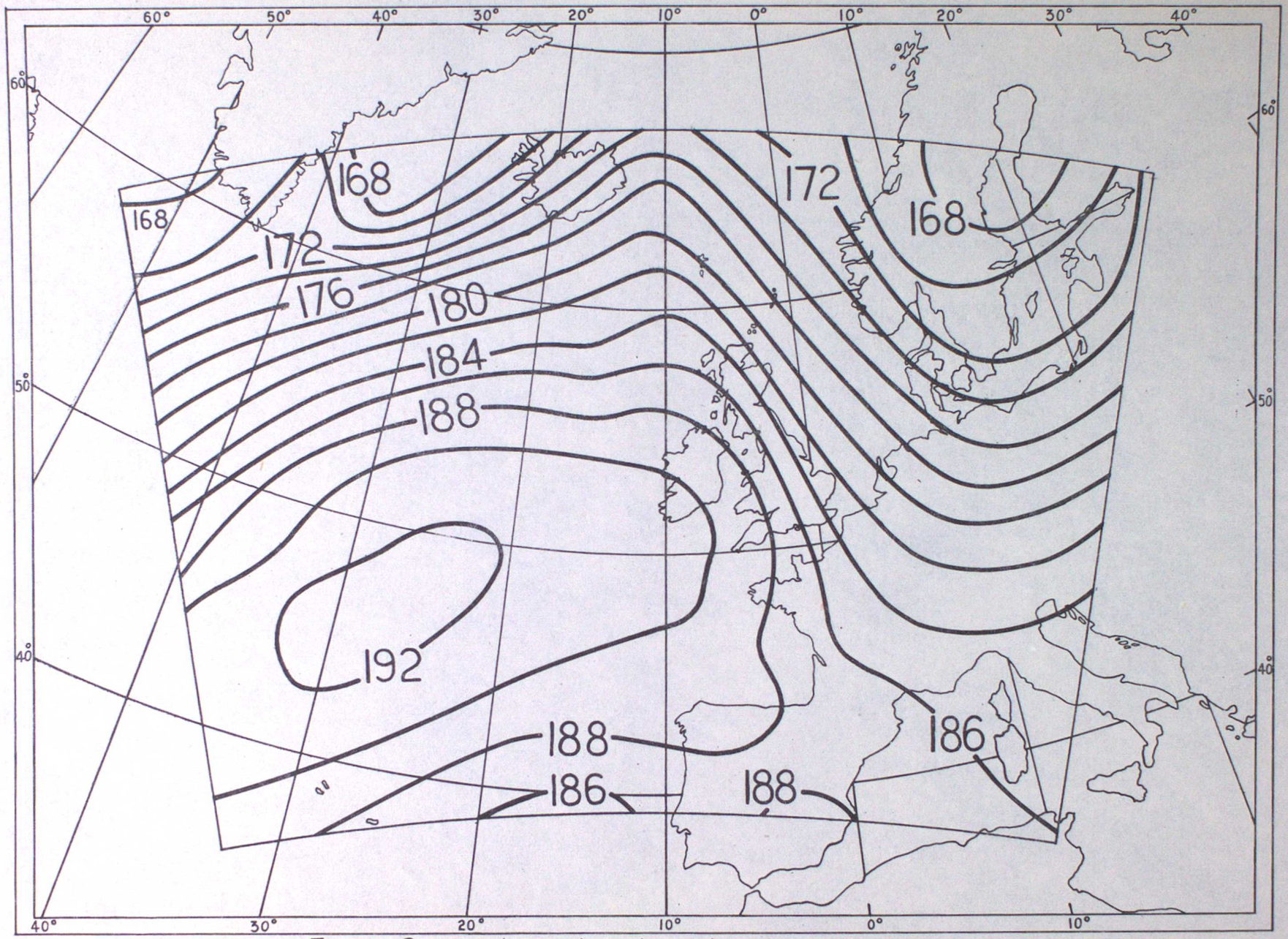

Fig. 9(b) Computed 500mb. contour chart for 0900 G.M.T. 15.3.49

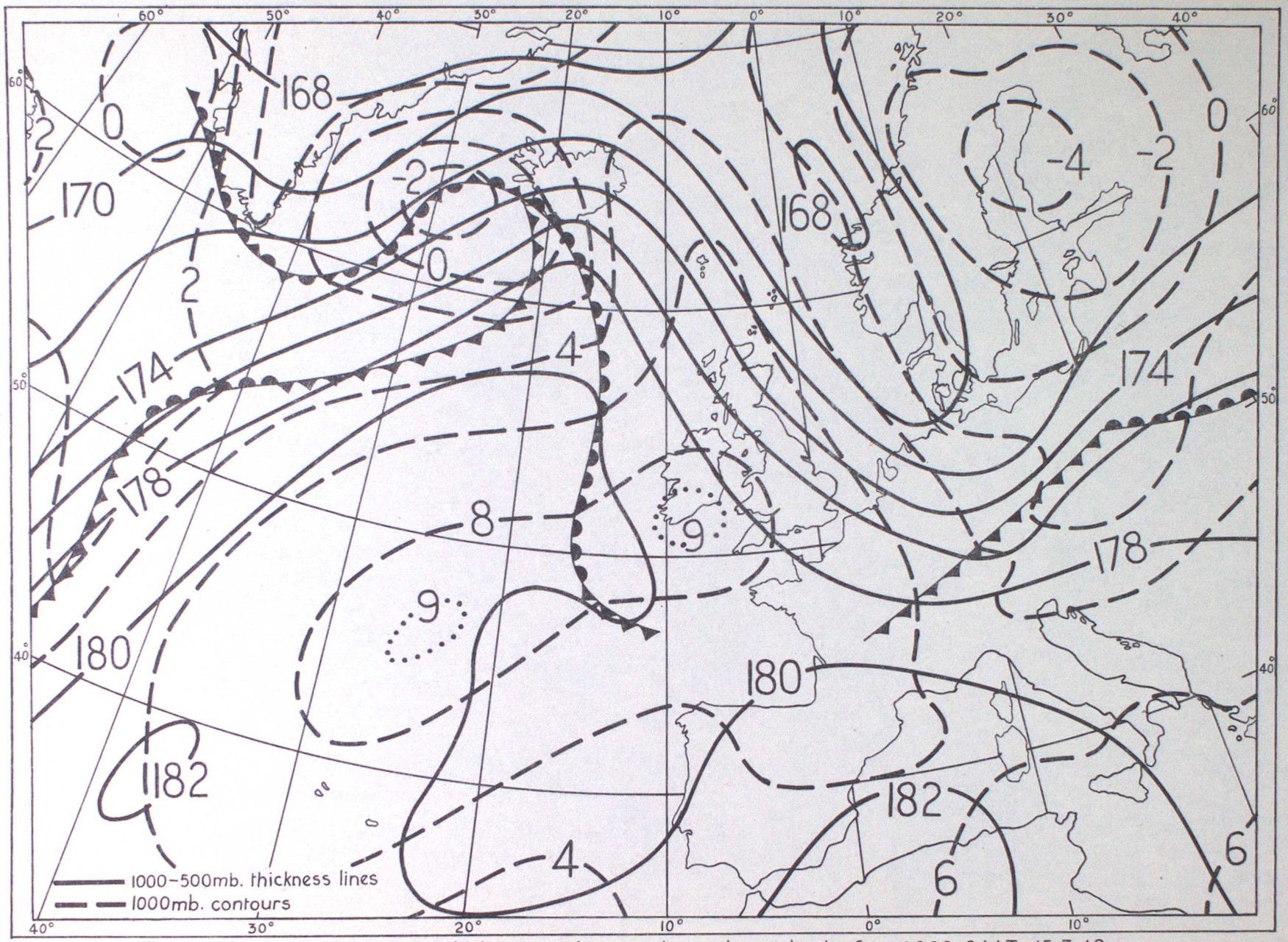

Fig. 9(c) Actual 1000–500mb. thickness and 1000mb. contour charts for 0900 G.M.T. 15.3.49

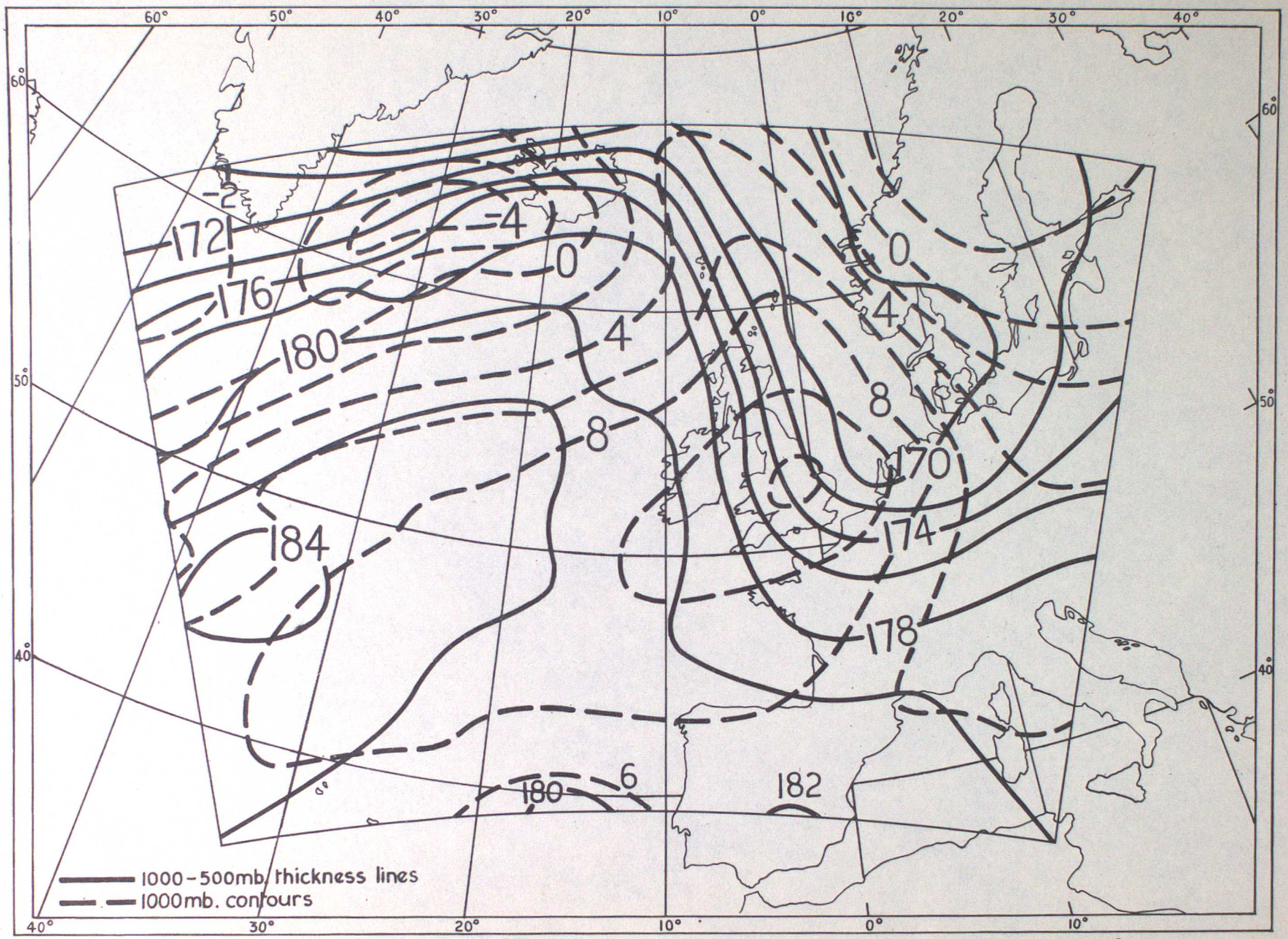

Fig. 9(d) Computed 1000-500mb. thickness and 1000mb. contour charts for 0900 G.M.T. 15.3.49

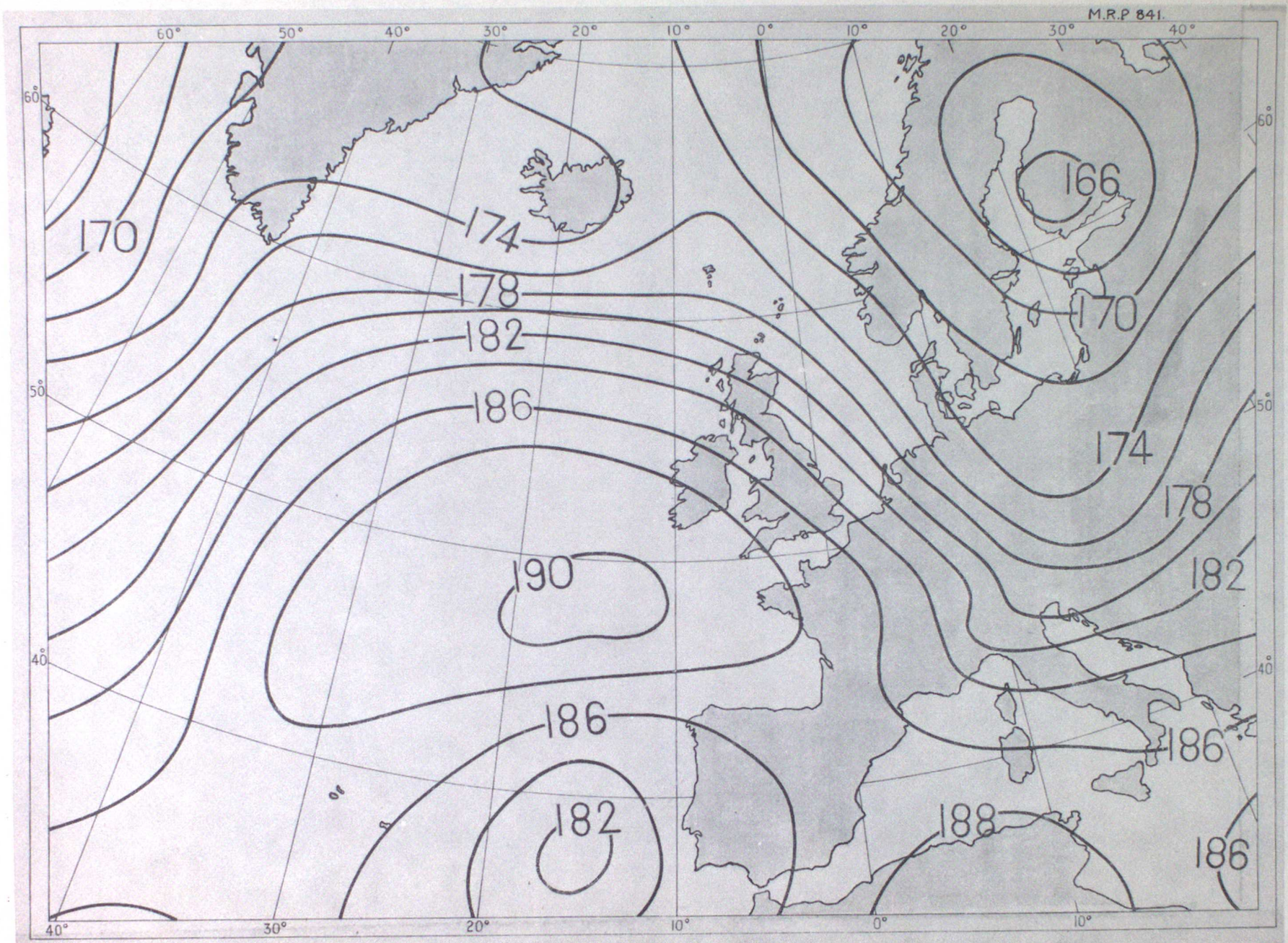

Fig. 10(a) Actual 500mb. contour chart for 1500 G.M.T. 15.3.49

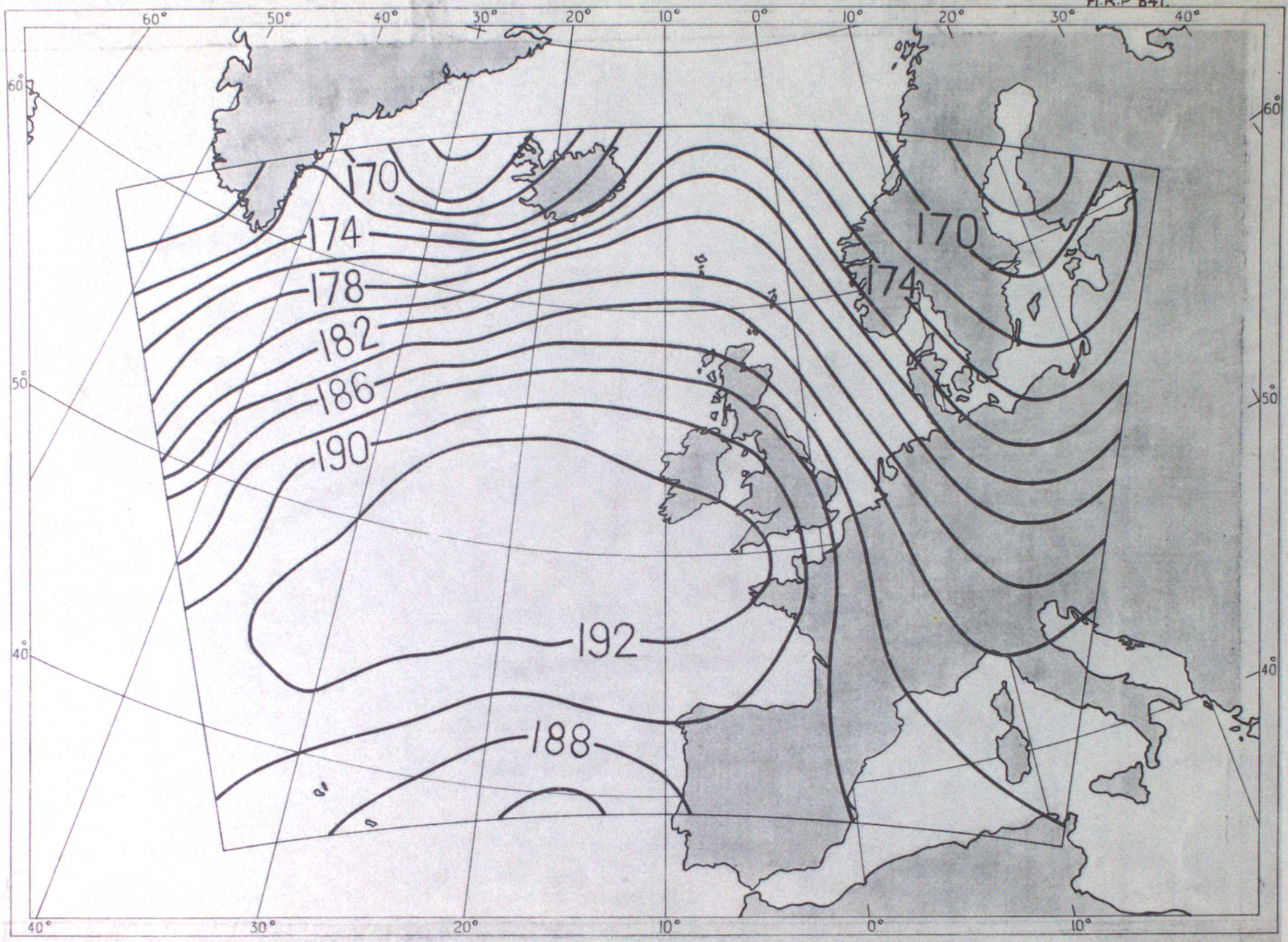

Fig.10(b) Computed 500mb. contour chart for 1500 G.M.T. 15.3.49

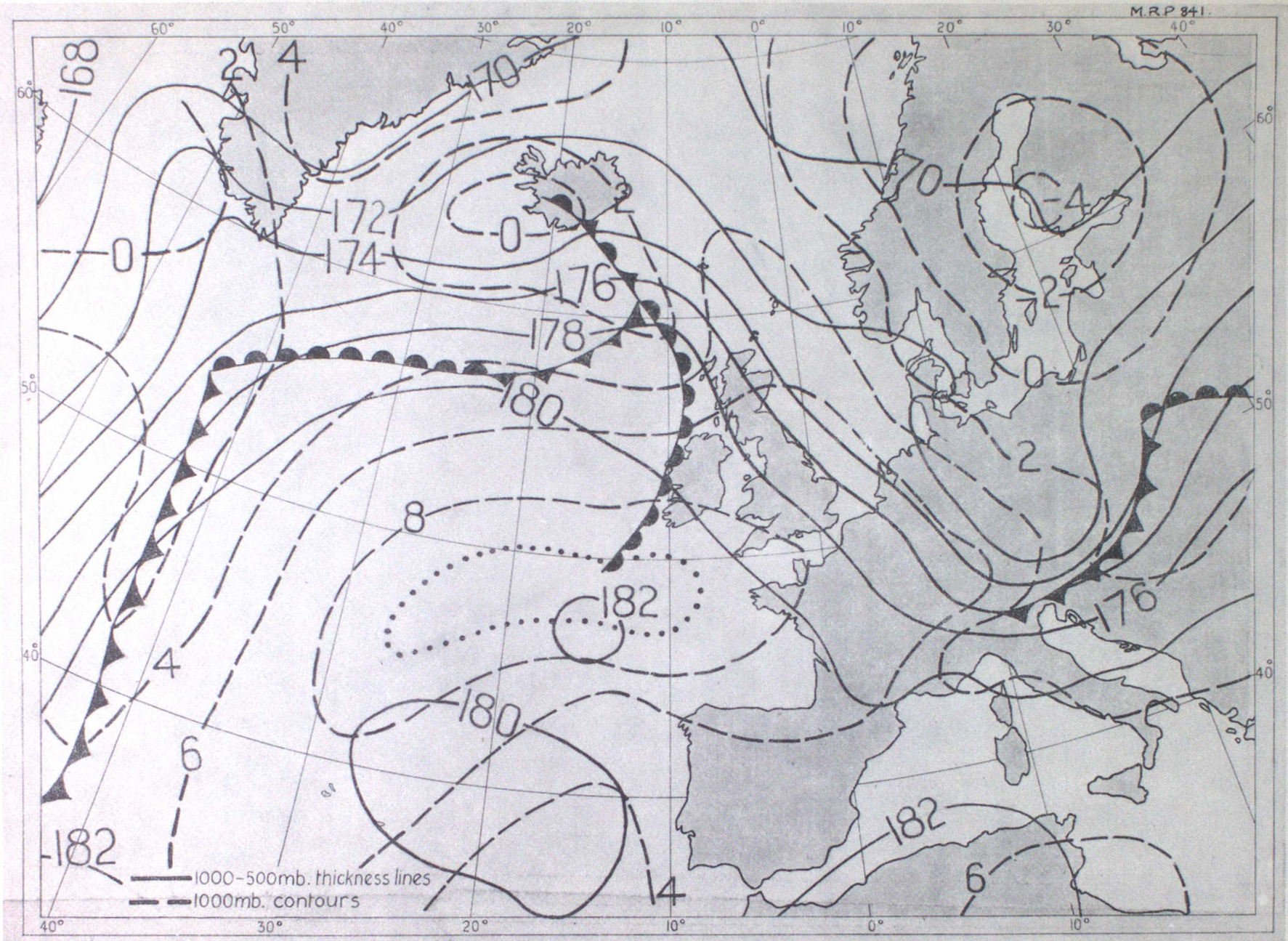

Fig.10(c) Actual 1000-500mb. thickness and 1000mb. contour charts for 1500 G.M.T. 15.3.49

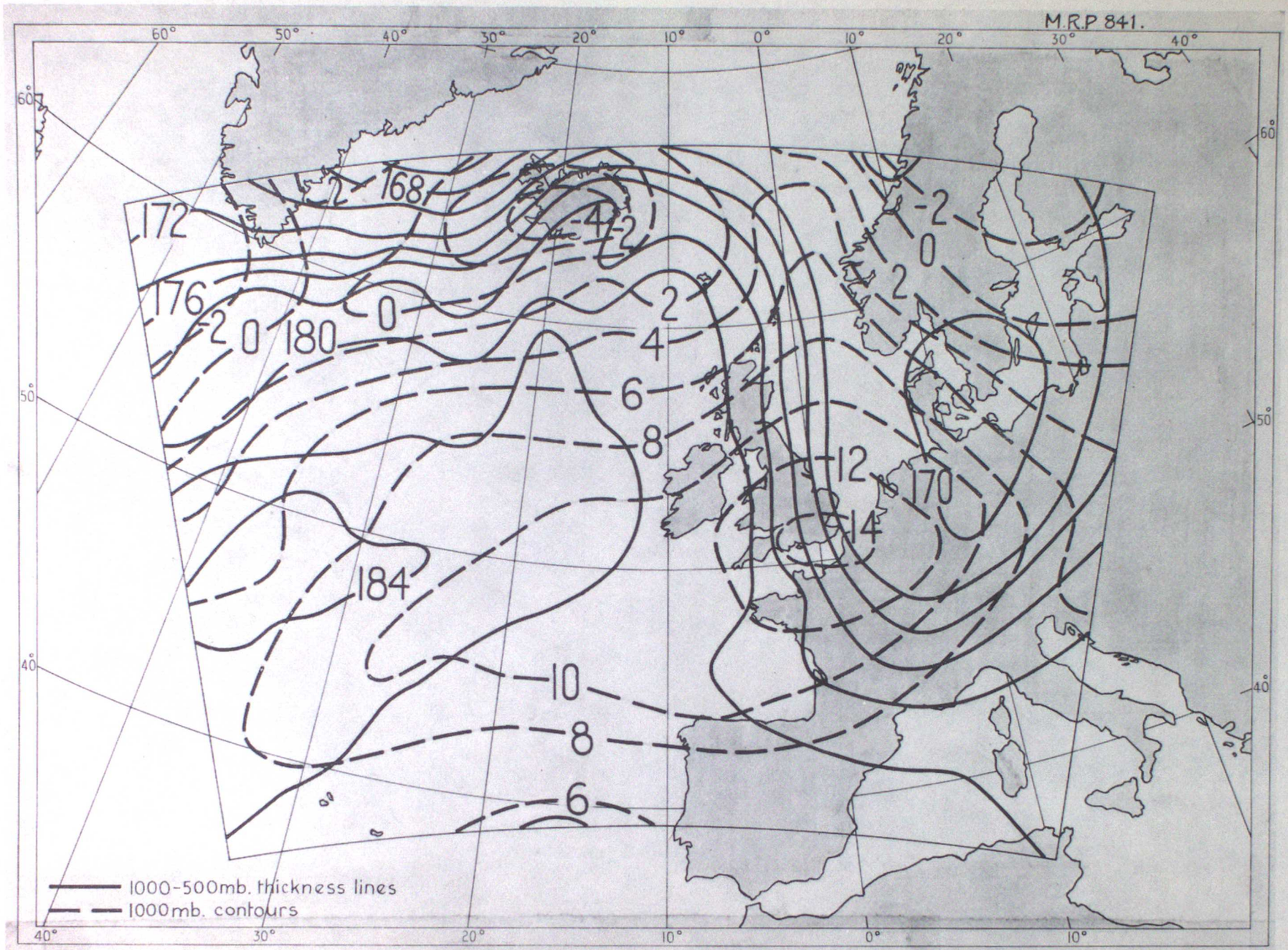

Fig. 10(d) Computed 1000–500mb. thickness and 1000mb. contour charts for 1500 G.M.T. 15.3.49